Atmos. Meas. Tech. Discuss., doi:10.5194/amt-2016-145, 2016
Manuscript under review for journal Atmos. Meas. Tech.
Published: 23 June 2016

Atmospheric Measurement Techniques
Discussions

A Bayesian model to correct underestimated 3D wind speeds from sonic anemometers increases turbulent components of the surface energy balance

John M. Frank[1,2], William J. Massman[1], and Brent E. Ewers[2]

[1]U.S. Forest Service, Rocky Mountain Research Station, 240 W. Prospect Rd., Fort Collins, CO, 80526

[2]University of Wyoming, Department of Botany and Program in Ecology, 1000 E. University Ave, Laramie, WY, 82071

*Corresponding author: telephone: +1 970 498 1319; email: jfrank@fs.fed.us

To be summited to Atmospheric Measurement Techniques

Atmos. Meas. Tech. Discuss., doi:10.5194/amt-2016-145, 2016
Manuscript under review for journal Atmos. Meas. Tech.
Published: 23 June 2016

Abstract

Sonic anemometers are the principal instruments in micrometeorological studies of turbulence and ecosystem fluxes. Recent studies have shown that common designs underestimate vertical wind measurements because they lack a correction for transducer shadowing, with no consensus on a suitable correction. We reanalyze a subset of data collected during field experiments in 2011 and 2013 featuring two or four CSAT3 sonic anemometers. We introduce a novel Bayesian analysis with the potential to resolve the three-dimensional correction by optimizing differences between anemometers mounted both vertically and horizontally. A grid of 512 points (~ ±5° resolution in wind location) is defined on a sphere around the sonic anemometer, from which the shadow correction for each transducer-pair is derived from a set of 138 unique state variables. Using the Markov chain Monte Carlo (MCMC) method, the Bayesian model proposes new values for each state variable, recalculates the fast-response dataset, summarizes the five-minute wind statistics, and accepts the proposed new values based on the probability that they make measurements from vertical and horizontal anemometers more equivalent. MCMC chains were constructed for three different prior distributions describing the state variables: no shadow correction, the Kaimal correction for transducer shadowing, and double the Kaimal correction, all initialized with 10% uncertainty. The final posterior correction did not depend on the prior distribution and revealed both self- and cross-shadowing effects from all transducers. After correction, the vertical wind velocity and sensible heat flux increased ~10% with ~2% uncertainty, which was significantly higher than the Kaimal correction. We applied the posterior correction to eddy covariance data from various sites across North America and found that the turbulent components of the energy balance (sensible plus latent heat flux) increased on average between 8-12%, with an average 95% credible interval between 6-14%. Considering this

is the most common sonic anemometer in the AmeriFlux network and is found widely within FLUXNET, these results provide a mechanistic explanation for much of the energy imbalance at these sites where all terrestrial/atmospheric fluxes of mass and energy are likely underestimated.

Atmos. Meas. Tech. Discuss., doi:10.5194/amt-2016-145, 2016
Manuscript under review for journal Atmos. Meas. Tech.
Published: 23 June 2016

1. Introduction

The eddy-covariance technique has become the most commonly used method for measuring the ecosystem exchange of mass and energy with the atmosphere. It is fundamental to the global network of flux towers that are central to quantifying terrestrial carbon sinks and sources (Baldocchi, 2003), to hydrological studies accounting for evapotranspiration and sublimation (Biederman et al., 2014; Reba et al., 2012), and to the energy balance through the turbulent fluxes of sensible and latent heat (Welch et al., 2015; Anderson and Wang, 2014). There is a growing consensus within the flux community that many sonic anemometers, the core instrument for all modern eddy-covariance systems, exhibit systematically biased underestimates of the vertical wind component (Frank et al., 2016; Horst et al., 2015; Kochendorfer et al., 2012). The ramifications for this are that all vertical fluxes (i.e., carbon dioxide, water vapor, latent heat, sensible heat, momentum) are similarly underestimated for any ecosystem. This is roughly consistent with the persistent energy balance closure problem across flux sites (Leuning et al., 2012; Stoy et al., 2013; Wilson et al., 2002) where a vast majority are assumed to be systematic biased towards low turbulent fluxes of sensible and latent heat.

Recent studies of Horst et al. (2015) and Frank et al. (2016) have shown that the error in at least two non-orthogonal sonic anemometer designs can be traced to transducer shadowing that remains uncorrected in the anemometer's firmware. In both studies, shadowing was described a priori by theoretical formulations based on the wind-tunnel tests of Kaimal (1979), yet there was no consensus on a correction. A shortcoming in the use of formulations derived for single transducer-pairs in laminar flow to describe turbulent flow distortions around more complex geometries (Fig. 1) is that shadowing between all transducers and structures cannot be accurately represented or incorporated. A second problem is that in turbulent flow fields there

Atmos. Meas. Tech. Discuss., doi:10.5194/amt-2016-145, 2016
Manuscript under review for journal Atmos. Meas. Tech.
Published: 23 June 2016

are few standards available to use as a calibration reference. Advancements in Bayesian techniques (Gelman et al., 2004) have created the potential to resolve both of these issues by incorporating prior knowledge of transducer flow distortions with a model that evaluates the omnidirectionality of a sonic anemometer to produce a posterior 3D correction.

To quantify a 3D correction of the CSAT3 sonic anemometer, we reanalyze data from field experiments conducted by Frank et al. (2013) and Frank et al. (2016) where wind measurements from non-orthogonal anemometers mounted vertically and horizontally were significantly different. We develop a Bayesian hierarchical model to evaluate three hypotheses:

(1) A 3D shadowing correction based solely on wind location can make a non-orthogonal sonic anemometer omnidirectional.

(2) This correction increases vertical wind measurements more than expected from single transducer shadowing because it accurately represents all shadowing between transducers.

(3) In ecosystems where these instruments are deployed, the application of this correction will result in significantly higher turbulent components of the energy budget and improved surface energy budget closure.

2 Methods

2.1 Reanalysis of field experiments

We reanalyze data from field campaigns conducted by Frank et al. (2013) and Frank et al. (2016). To summarize them, experiments were conducted in 2011 and 2013 where multiple sonic anemometers were deployed in a horizontal array at 24.5 m height on the Glacier Lakes Ecosystem Experiments Site (GLEES) AmeriFlux scaffold above a subalpine forest in southeastern Wyoming, USA (Frank et al., 2014). The anemometers were initially mounted

Atmos. Meas. Tech. Discuss., doi:10.5194/amt-2016-145, 2016
Manuscript under review for journal Atmos. Meas. Tech.
Published: 23 June 2016

vertically, oriented west, arranged south to north, staggered up and down, and located 0.50 m center-to-center from each other (Fig. 1). Periodically, some of the anemometers were rotated 90° around their *u*-axis and mounted horizontally. In this study we focus only on the CSAT3 sonic anemometer (Campbell Scientific, Inc., Logan, UT, USA) during times when both vertically and horizontally mounted anemometers were present (Table 1). It is conventional to describe the three dimensions of a sonic anemometer as the *u*, *v*, and *w*-axes. To reduce confusion in describing horizontal anemometers, we refer to cardinal *u*, *v*, and *w* where the measurements have been rotated to west-east (*u*), south-north (*v*), and down-up (*w*), which are consistent with *u*, *v*, and *w* for vertically mounted anemometers. Finally, because our Bayesian model is computationally intensive we reanalyze a subset of only 5% of the available data (see section 2.3).

2.2 The Bayesian model

Bayesian statistics are based on Bayes theorem (Bayes and Price, 1763), which in modern applications relates the posterior probability of a model parameter conditioned on data to the product of the likelihood of the data and the prior probability of that parameter (Gelman et al., 2004). In essence, the prior represents an initial educated guess or belief in the value of a model parameter, the likelihood is the probability of observing the data if it was deterministically generated from a model, and the posterior is an updated belief in the model parameter considering each the prior, the model, and the data. Analytical evaluation of the posterior is rarely possible, as is in our case, thus the posterior is commonly estimate through the Markov chain Monte Carlo (MCMC) method, Gibbs sampling (Appendix A.1), and the Metropolis-Hastings algorithm (Kruschke, 2010). The framework of our Bayesian model is to divide the sphere around the sonic anemometer into approximately equal grid points and to define a prior

Atmos. Meas. Tech. Discuss., doi:10.5194/amt-2016-145, 2016
Manuscript under review for journal Atmos. Meas. Tech.
Published: 23 June 2016

probability distribution of the 3D shadowing correction for each transducer pair at each location. Then, the model proposes new corrections for each grid point, recalculates the fast-response dataset, summarizes new five-minute wind statistics, determines the probability that the updated measurements from vertical and horizontal anemometers are more equivalent using the proposed correction versus the old one (i.e., the ratio of Eq. A13 evaluated for the proposed versus old correction), and finally accepts/rejects the proposal probabilistically from this ratio to construct the posterior correction. The model recursively adjusts the distribution that generates the proposals to achieve between 25 and 50% acceptance rates. We define a grid of 512 points (~ ±5° resolution of wind location) on a sphere around each of the three transducer pairs of the sonic anemometer. Neglecting the upper and lower mounting arms that extend back into the electronics housing and support block, the CSAT3 is symmetrical on either side of a transducer pair, between the upper and lower hemispheres, and for each of the three transducer pairs. To pool data and reduce computations, we make these assumptions of symmetry to describe all 1,536 points from a set of 138 unique state variables.

We test three prior corrections: no shadow correction, the Kaimal correction (Kaimal, 1979; Frank et al., 2016; Horst et al., 2015), and a doubling of the Kaimal correction (Frank et al., 2016). The Kaimal correction is defined as $U_c = (1 - 0.16 + 0.16\theta/70)\acute{U}_C$ for $\theta \leq 70°$ and $U_c = \acute{U}_C$ for $\theta > 70°$, where U_C and $\acute{U}_C$ are the measured and corrected wind velocities and θ is the angle between the wind and the acoustic path.

The model predicts the standard deviation of the data, $\sigma_{f,i,c}$, during each five-minute period, *f*, for each replicate sonic anemometer, *i*, in the three cardinal dimensions, *c* (Fig. 1), from a normal distribution with mean $\hat{\sigma}_{f,i,c}$ and standard deviation ε (Eq. 1).

$$\sigma_{f,i,c} \sim \mathrm{N}\left(\hat{\sigma}_{f,i,c}, \varepsilon^{-2}\right) \quad (1)$$

Atmos. Meas. Tech. Discuss., doi:10.5194/amt-2016-145, 2016
Manuscript under review for journal Atmos. Meas. Tech.
Published: 23 June 2016

Atmospheric Measurement Techniques
Discussions

The predicted mean is constructed in several steps. First, the state variable for the 3D correction, $\vec{\alpha}_{T\times G}$, is a matrix representing each of the three transducer axes, t, for each grid point, g. Here it does not matter if each grid point is independent or that they linked together through symmetry. It is given a normal prior probability distribution with mean equal to the prior correction, $P_{t,g}$, evaluated for each transducer-pair for wind blowing through the longitude, λ, and latitude, φ, associated with each grid point with a predefined standard deviation equal to 0.1, or ±10% uncertainty (Eq. 2).

$$\alpha_{T\times G_{t,g}} \sim \mathrm{N}\left(P_{t,g}, 0.1\right) \tag{2}$$

The 3D correction is applied to every 20-Hz sample, j, of the original measured wind velocity data in transducer coordinates, $U_{T_{t,f,i,j}}$. The multidimensional nominal predictor variable, $\vec{x}_{G\times F\times I\times J_{g,f,i,j}}$, selects the corresponding grid point that occurs with every 20-Hz sample. The corrected 20-Hz wind velocity in transducer coordinates is $\acute{U}_{T_{t,f,i,j}}$ (Eq. 3).

$$\acute{U}_{T_{t,f,i,j}} = U_{T_{t,f,i,j}} \cdot \left(\vec{\alpha}_{T\times G}\vec{x}_{G\times F\times I\times J_{g,f,i,j}}\right) \tag{3}$$

The non-orthogonal data is transformed via matrix multiplication into orthogonal coordinates, $\acute{U}_{S_{s,f,i,j}}$, with the three sonic dimensions, s (Eq. 4).

$$\acute{U}_{S_{s,f,i,j}} = \vec{M}_{S\times T}\acute{U}_{T_{t,f,i,j}} \tag{4}$$

The matrix, $\vec{M}_{S\times T}$, is specific to the CSAT3 geometry (Eq. 5).

$$\vec{M}_{S\times T} = \begin{bmatrix} -\frac{4}{3} & \frac{2}{3} & \frac{2}{3} \\ 0 & \frac{2}{\sqrt{3}} & -\frac{2}{\sqrt{3}} \\ \frac{2}{3\sqrt{3}} & \frac{2}{3\sqrt{3}} & \frac{2}{3\sqrt{3}} \end{bmatrix} = \begin{bmatrix} -1.333 & 0.667 & 0.667 \\ 0 & 1.155 & -1.155 \\ 0.385 & 0.385 & 0.385 \end{bmatrix} \tag{5}$$

In order for the model to predict data simultaneously from both vertical and horizontal anemometers, a final corrected time series data set is produced in cardinal coordinates, $\acute{U}_{C_{f,i,c,j}}$.

Atmos. Meas. Tech. Discuss., doi:10.5194/amt-2016-145, 2016
Manuscript under review for journal Atmos. Meas. Tech.
Published: 23 June 2016

Atmospheric Measurement Techniques
Discussions

$$\acute{U}_{C_{f,i,c,j}} = \left(\vec{x}_{F\times I\times J\times O_{f,i,j,o}} \vec{N}_{O\times C\times S}\right) \acute{U}_{S_{S,f,i,j}} \tag{6}$$

The matrix $\vec{N}_{O\times C\times S}$ is straightforward (Eq. 7), and the multidimensional nominal predictor variable, $\vec{x}_{F\times I\times J\times O_{f,i,j,o}}$, selects the orientation, o, of every 20-Hz sample.

$$\vec{N}_{O\times C\times S} = \begin{cases} \begin{bmatrix} 1 & 0 & 0 \\ 0 & 1 & 0 \\ 0 & 0 & 1 \end{bmatrix}, & o = 1\ (i.e, vertical) \\ \begin{bmatrix} 1 & 0 & 0 \\ 0 & 0 & -1 \\ 0 & 1 & 0 \end{bmatrix}, & o = 2\ (i.e., horizontal) \end{cases} \tag{7}$$

Using the corrected time series data in cardinal coordinates, the model calculates the average correction, $\beta_{F\times I\times C_{f,i,c}}$, for the five-minute standard deviation data for each anemometer in each dimension (Eq. 8).

$$\beta_{F\times I\times C_{f,i,c}} = \frac{\sqrt{\frac{1}{J-1}\sum_{j=1}^{J}\left(\acute{U}_{C_{f,i,c,j}} - \frac{1}{J}\sum_{j=1}^{J}\acute{U}_{C_{f,i,c,j}}\right)^2}}{\sqrt{\frac{1}{J-1}\sum_{j=1}^{J}\left(U_{C_{f,i,c,j}} - \frac{1}{J}\sum_{j=1}^{J}U_{C_{f,i,c,j}}\right)^2}} \tag{8}$$

Eq. 8 is equivalent to the ratio of the standard deviation of $\acute{U}_C$ divided by the standard deviation of U_C evaluated during each five-minute period for each sonic anemometer in each cardinal dimension. The reference condition for every five-minute period, $\vec{\tilde{\sigma}}_{F\times C}$, is a state variable representing the "true" standard deviation of wind velocity in each cardinal dimension. It is assigned a uniform prior probability distribution that generously includes the "true" value by allowing each $\tilde{\sigma}_{F\times C}$ to range from 0 to the maximum of all U_C measurements (Eq. 9).

$$\tilde{\sigma}_{F\times C_{f,c}} \sim Unif\left(0, max(U_C)\right) \tag{9}$$

Finally, the model predicts the mean for the standard deviation data as the reference divided by the correction (Eq. 10).

$$\hat{\sigma}_{f,i,c} = \frac{\vec{\tilde{\sigma}}_{F\times C} \cdot \vec{x}_{F\times C_{f,c}}}{\vec{\beta}_{F\times I\times C} \cdot \vec{x}_{F\times I\times C_{f,i,c}}} \tag{10}$$

Atmos. Meas. Tech. Discuss., doi:10.5194/amt-2016-145, 2016
Manuscript under review for journal Atmos. Meas. Tech.
Published: 23 June 2016

The nominal predictor variable, $\vec{x}_{F\times C_{f,c}}$, selects the appropriate five-minute reference for each cardinal dimension while the other nominal predictor variable, $\vec{x}_{F\times I\times C_{f,i,c}}$, selects the five-minute correction for each sonic anemometer for that dimension.

To complete the Bayesian model definition, the model error is a state variable which is assigned a prior probability distribution with a gamma distribution (Eq. 11).

$$\varepsilon \sim \mathrm{Gamma}\left(1, \acute{b}\right) \tag{11}$$

The variance of the gamma distribution, $\acute{b}$, is assigned the same variance as the prior distribution for $\tilde{\sigma}_{F\times C}$ which is a uniform distribution (Eq. 12).

$$\acute{b} = \frac{\sqrt{12}}{max(U_C)-0} \tag{12}$$

Distributions are defined where normal distributions are $\theta \sim \mathrm{N}(a, b)$ with expected value $\mathrm{E}(\theta) = a$ and variance $\mathrm{var}(\theta) = 1/b^2$, gamma distributions are $\theta \sim \mathrm{Gamma}(a, b)$ with $\mathrm{E}(\theta) = a/b$ and $\mathrm{var}(\theta) = a/b^2$, and uniform distributions are $\theta \sim \mathrm{Unif}(a, b)$ with $\mathrm{E}(\theta) = (a+b)/2$ and $\mathrm{var}(\theta) = (b-a)^2/12$.

2.3 Analysis

Our Bayesian analysis was conducted using R (version 3.2.2, (R Core Team, 2015)) within RStudio (version 0.99.486, (RStudio Team, 2015)). We constructed an MCMC chain of 10,000 steps for each of the three priors. Because the Bayesian model estimates are relative and not an absolute correction (see discussion in section 4.1), we normalized each chain. This was done in post-processing by dividing each update to the 138 unique corrections by the average correction across all grid points. We inspected each chain and removed the first 500 steps for burn-in and kept 1 out of every 140 steps to eliminate autocorrelation between steps for most grid points (even after reducing to 138 state variables, a few of these were estimated from relatively little data which unavoidably led to high autocorrelation between steps). This reduced each MCMC chain to 68 steps, which we combined between the three priors to create a single

Atmos. Meas. Tech. Discuss., doi:10.5194/amt-2016-145, 2016
Manuscript under review for journal Atmos. Meas. Tech.
Published: 23 June 2016

chain containing 204 independent samples of the posterior distribution of the normalized 3D correction. To define an absolute correction such that equatorial measurements (i.e., $(u^2 + v^2)^{½}$) are unchanged (see discussion in section 4.1), we applied the normalized correction to the time series data of vertically mounted anemometers, calculated the corrected five-minute standard deviations for equatorial winds, performed linear regression without an intercept (i.e., model the average change in equatorial winds solely as a scaling factor) between these corrected and uncorrected standard deviations for each of the 204 posterior samples, and determined the scaling factor as the average of the 204 regression slopes. We divided all values in the normalized 3D correction by this scaling factor to produce our final posterior correction.

Computation of the Bayesian model was extremely intensive: completion of the three chains took upwards of two months of continuous computer processing (Windows 7, Intel® Core™ i7-3630QM CPU @ 2.40 GHz processor, 1 TB solid state hard drive, 20 GB RAM). During beta testing we attempted to estimate the 3D correction independently for all grid points and all transducer pairs, with a single MCMC chain requiring a half-year to complete. Likewise, we investigated increasing the number of grid points to obtain better resolution around the sphere as well as increasing the amount of sonic anemometer data used from the Frank et al. (2013) and Frank et al. (2016) datasets. In both cases we desired an order of magnitude better resolution or more data, but the time required to complete a single MCMC chain quickly made these improvements impractical. Instead, we determined that 512 grid points and 5% of the original data was optimal considering these processing constraints.

There is a slight distinction to be made between the prior corrections which are defined as a function, $\alpha(\lambda, \varphi)$, of the true longitude and latitude of the wind and the posterior correction which is a function, $\alpha(\tilde{\lambda}, \tilde{\varphi})$, where ~ represents the uncorrected sonic anemometer measurement of wind location. This means the posterior correction can be applied directly to the uncorrected data whereas the prior should be applied recursively (i.e., determine the correction, update the wind location, update the correction). To directly compare the prior and posterior corrections, we also present our posterior correction with the wind locations recursively adjusted to approximate the "true" longitude and latitude. For these analyses, we smoothed the posterior with a spherical spline fit (Wahba, 1981) using R package mgcv (Wood, 2006).

We quantified the impact of shadowing on measurements of the standard deviations of winds in the three dimensions and the sensible heat flux (*H*). This was done by applying the posterior correction to the time series data of vertically mounted anemometers, calculating the five-minute measurements, performing linear regression without an intercept between the corrected and uncorrected measurements for each of the 204 posterior samples, and defining the impact as a distribution composed of the 204 regression slopes. For *H*, the data was planar fit rotated (Lee et al., 2004), time lag adjusted, and vapor flux corrected (Massman and Lee, 2002) using ancillary data from the GLEES AmeriFlux site (Frank et al., 2014).

Finally, we quantified the impact of the 3D correction on the sum of the turbulent components of the energy balance (i.e., sensible and latent (*LE*) heat flux) at various sites across North America (Table 2). Each site featured a CSAT3, a fast-response hygrometer, and ancillary meteorological data. Measurements of *LE* were calculated similar to *H* but including the Webb-Pearman-Leuning correction (Webb et al., 1980). The impact of the 3D correction was quantified as a distribution similar to above, except compiled from 30-minute time periods.

3 Results

3.1 No correction

Atmos. Meas. Tech. Discuss., doi:10.5194/amt-2016-145, 2016
Manuscript under review for journal Atmos. Meas. Tech.
Published: 23 June 2016

Atmospheric Measurement Techniques
Open Access
Discussions

Without any shadow correction applied, measurements between a vertically and a horizontally mounted anemometer were different, which becomes clear when the variance between two vertical anemometers is taken into account (Fig. 2b, d, f versus a, c, e). The root mean square error (RMSE) in the 5-minute standard deviation of wind along all cardinal dimensions (u, v, and w) combined was 9.4% between a vertical and a horizontal anemometer, whereas the same metric between two vertical anemometers was 3.9%. The largest discrepancy was along the cardinal v-axis, where the RMSE increased from 3.7% to 11.1% when comparing vertical and horizontal anemometers (Fig. 2c versus d).

3.2 The Kaimal prior correction

The Kaimal correction is symmetrical with respect to each sonic transducer path (Fig. 3a, c, e). Yet, the same correction when viewed in sonic coordinates reveals unique responses for u, v, and w (Fig. 3b, d, f). For small latitude winds, the corrections are small for u and v measurements, while those for w are higher yet unstable around the equator (see discussion in section 4.2). When the Kaimal correction was applied to the vertically mounted anemometers, there were minor increases in the 5-minute standard deviations of u and v (0.8% and 2.9%) while the increases for w (5.6%) and H (5.5%) were more substantial. This correction explained some of the differences between vertically and horizontally mounted anemometers (Fig. 4) where the RMSE for all cardinal dimensions combined was 6.2%, or 1.60 times greater than the same error between two vertical anemometers. The discrepancy along the cardinal v-axis decreased to 6.6%, or 1.86 times greater than the same error for two vertical anemometers, though some bias is still apparent (Fig. 4c versus d). While the Kaimal correction is only one of three priors tested in our Bayesian model, it is perhaps the most accepted algorithm currently available to correct transducer shadowing in the CSAT3.

3.3 The Bayesian model

Figure 5 illustrates the approach of the Bayesian model. The model initializes the 512 grid points with a prior, in this case the Kaimal correction. No matter the transducer pair or vertical versus horizontal mounting, the 3D correction for all cases are identical but rotated versions of a common correction based on 138 unique state variables. For a single instantaneous wind, the simultaneous corrections for all six combinations of transducer pairs and mounting orientations will be different. As the MCMC chains progress, the Bayesian model will continuously adjust each of the 138 unique state variables so that measurements from the vertically and horizontally mounted anemometers are most similar based on the univariate conditional posterior probability distribution (Eq. A13). Much of the predictive power of the model comes from resolving the inconsistencies along the cardinal *v*-axis (Fig. 2d) where vertically and horizontally mounted anemometers are likely to be most dissimilar. Specifically, a vertically mounted CSAT3 should measure reasonably correct cross winds which must flow across the entire transducer and support structure of a horizontally mounted CSAT3.

Each MCMC chain was initialized with the mean of each prior, yet after convergence their posterior corrections were remarkably similar regardless of the choice of prior correction, with one peculiarity (Fig. 6). There was a clear linear relationship between the prior correction averaged across all 512 grid points (1.000 for no correction, 1.040 for the Kaimal correction, and 1.080 for the double-Kaimal correction) and the magnitude of the posterior correction (1.030, 1.064, and 1.098, respectively) that relates to the Bayesian model estimating a relative and not absolute correction (see discussion in section 4.1). The posterior correction is more than an estimate of the optimal solution, as it intrinsically accounts for the uncertainty of the correction at each of the 512 grid points (Fig. 7). Whereas each prior was defined with 10% uncertainty

Atmos. Meas. Tech. Discuss., doi:10.5194/amt-2016-145, 2016
Manuscript under review for journal Atmos. Meas. Tech.
Published: 23 June 2016

Atmospheric Measurement Techniques
Discussions

(Eq. 2), much of the posterior correction has much lower standard deviations, especially around the transducers where values were as low as 2.5% (Fig. 7a). These uncertainties can be expressed in sonic coordinates for the u, v, and w components, which in general show that the posterior correction is most certain for winds along each of those axes, respectively (Fig. 7b-d), with the uncertainty along the w measurement ranging from 2.7-18.3%.

Figure 8 illustrates the completion of the Bayesian model where the same posterior correction is applied to all transducer pairs and both mounting orientations. For every instantaneous wind, application of these six different corrections ultimately results in the 5-minute standard deviations of wind along the cardinal u, v, and w axis being most similar between the two mounting orientations.

3.4 The posterior correction

The posterior correction for each transducer pair is presented in Figure 9. These results take into account the recursive adjustment to the wind locations and have been smoothed with a spherical spline. Significantly more self-shadowing and cross-shadowing around the transducers is visible than compared to the Kaimal prior (Fig. 9a, c, e versus Fig. 3a, c, e, in locations near all transducers). These results are more certain (i.e., low standard deviations when compared to the original 10% assigned to the prior) near the transducers, poorly constrained near the equator (Fig. 7a), and independent of the choice of prior correction (Fig. 6). Transforming the posterior correction into sonic coordinates reveals that similar to the Kaimal prior, minimal u and v correction is required for small latitude winds (Fig. 9b, d versus 3b, d). But, the impact of the additional transducer shadowing impacts w measurements far more than was predicted (Fig. 9f versus Fig. 3f) where the posterior was fairly certain for latitudes greater than ±13.5° (Fig. 7d); the high uncertainty for near-equatorial wind is discussed in Sect. 4.2. The posterior corrected

Atmos. Meas. Tech. Discuss., doi:10.5194/amt-2016-145, 2016
Manuscript under review for journal Atmos. Meas. Tech.
Published: 23 June 2016

CSAT3 was the most omnidirectional between vertically and horizontally mounted anemometers (Fig. 10) where the RMSE for all cardinal dimensions combined was 5.3%, or 1.36 times greater than the same error between two vertical anemometers. The discrepancy along the cardinal *v*-axis was further reduced to 4.4%, which is only 1.20 times greater than the same error for two vertical anemometers, and the bias has been removed (Fig. 10d versus 4d). When the posterior correction was applied to the vertically mounted anemometers there were similar increases to the Kaimal correction in the 5-minute standard deviations of *u* and *v* (0.6 ± 0.8 [-1.0 2.2]%, 2.7 ± 0.7 [1.5 4.1]%, mean ± standard deviation [95% credible interval], Fig. 11a-b). But, compared to the Kaimal correction, the increases in *w* (10.6 ± 1.7 [7.6 13.9]%) and *H* (9.9 ± 1.6 [7.2 12.6]%) were substantial and significantly higher (Fig. 11c-d). We provide the MCMC chain for the final posterior correction in the supplementary material as a tool for researchers to evaluate in other sonic anemometer studies, to examine the uncertainty in ecosystem flux measurements, and to investigate surface energy balance closure.

3.5 Turbulent components of the ecosystem energy balance across a continent

We applied the posterior correction to various sites across North America that deploy the CSAT3 in their eddy-covariance instrumentation (Table 2). The estimated increase in *H* + *LE* at these sites ranged from 8.1-11.6% with an average standard deviation and 95% credible interval of ±1.9% and 6.1-13.8%. For all but one site, the increase in *H* + *LE* was significantly higher than the increase due to the Kaimal correction. At the 2 m Yuma, AZ site, the lack of significance is related to anomalously low instantaneous wind latitudes for which the *w* correction is most uncertain (Fig. 7d).

4 Discussion

4.1 An omnidirectional standard

Perhaps the most important shortcoming in almost every sonic anemometer study is the lack of a standard wind measurement to compare against. A fundamental problem is that the principle of sonic measurements (Barrett and Suomi, 1949; Kaimal and Businger, 1963) involves the observer effect, i.e. it is virtually impossible for sonic transducers to observe air parcels without influencing them (Buks et al., 1998). Thus, any method that relies on a sonic anemometer measurement as an absolute standard is flawed to an extent. And while we are justified to believe that some sonic anemometer measurements are more accurate that others (Frank et al., 2016) it is tenuous to choose any sonic anemometer measurement as a standard. Then, what are the alternatives? Wind tunnels are extremely useful (Horst et al., 2015; van der Molen et al., 2004) yet it is debatable that such laminar or quasi-laminar calibrations are transferrable to turbulent field conditions (Hogstrom and Smedman, 2004). And, while other new technologies such as Doppler Lidar exist (Sathe et al., 2011; Dellwik et al., 2015) their application as a field reference standard has been limited.

What we address is the general problem of determining a calibration given an unknown standard or nothing to compare against. Whether this problem exists in medicine (Lu et al., 1997), acoustics (MacLean, 1940; Monnier et al., 2012), or micrometeorology with respect calibrating sonic anemometry in turbulent flow fields, all approaches have a commonality of testing the relative consistency of a response to unknown signals. In our situation, we hold the 3D sonic anemometer to an omnidirectional standard of relative consistency and contend that the correction that best achieves this standard is statistically the most likely 3D calibration. A CSAT3 without any 3D shadow correction is clearly not omnidirectional (Fig 2) as measurements depend on the instrument's orientation. A CSAT3 with the Kaimal transducer shadow correction is better at meeting this standard (Fig 4). However, the posterior 3D correction is remarkably effective in making the CSAT3 omnidirectional (Fig. 10). Because the posterior correction closely achieves the omnidirectional standard, we support our first hypothesis and argue that it is the most accurate correction, in general, for the three dimensions of the CSAT3. Whether or not the posterior correction reveals meaningful information regarding vertical winds and turbulent fluxes is another matter discussed below.

A consequence of the omnidirectional standard is that implicitly this produces only relative results. Indeed, our Bayesian posterior has no meaning in an absolute sense without the additional constraint that equatorial winds should be unchanged by the correction. We do not specify the 3D correction at any of the grid points nor we do we specify a reference or “true” condition for the standard deviation of wind during any five minute period. Because of this, the parameter estimates for $\vec{\vec{\sigma}}_{F\times C}$ and $\vec{\alpha}_{T\times G}$ only have meaning relative to each other. This issue is confounded by the choice of prior distributions which vary dramatically in shape, but produce similar posteriors except for differences in their absolute magnitudes (Fig. 6), i.e., higher magnitude priors produce higher magnitude posteriors. Which absolute magnitude is correct? Without specifying an absolute standard, the answer is none of them. To facilitate comparison and combination of the posteriors we normalized the three MCMC chains.

There is a clear need to specify an absolute standard to reference our results. Without one, our normalized posterior correction reduced the 5-minute standard deviations for equatorial winds (i.e., the *u*-*v* plane) by 7%. Does this make physical sense? No. The idea that equatorial winds should not be changed is consistent with the expectation that the CSAT3 measures accurate equatorial winds, something that has been demonstrated in both wind tunnels and field campaigns (Yahaya and Frangi, 2004; Friebel et al., 2009). Even the Kaimal correction, which is an absolute correction, predicts <0.1% error in our measurements of equatorial winds. Because the omnidirectional standard is only relative, we impose an additional absolute standard by defining the average correction for equatorial winds to be zero, which is simply achieved by scaling the normalized posterior correction by 7%. While there certainly is some leeway in this constraint, if the normalized posterior correction were scaled by anything other than 7 ± 1.4% then the correction to horizontal winds would be significantly different (95% credible interval) than both zero and the Kaimal correction (Fig. 11a-b) and would run counter to our belief that the CSAT3 measures reasonable accurate horizontal winds.

4.2 Impact on vertical wind measurements and sensible heat flux

Recent studies have questioned the accuracy of CSAT3 vertical wind velocity measurements (Frank et al., 2013; Kochendorfer et al., 2012) culminating with Horst et al. (2015) and Frank et al. (2016) who identified the anemometer's lack of transducer shadowing correction as the root cause. Quantifying the inaccuracy and determining how to fix this problem has been a challenge. While each of these studies estimated different errors in w at their field sites (3.5% (Horst et al., 2015), 6-10% (Frank et al., 2013), 5.5-12.5% (Frank et al., 2016), and 14% (Kochendorfer et al., 2012)), it wasn't until Horst et al. (2015) proposed the application of the Kaimal correction (Kaimal, 1979) that a mechanistic explanation was used to quantify the underestimate. Whether or not the Kaimal correction is sufficient is a matter of debate, but it currently represents the best prior knowledge to explain the CSAT3's shortcomings.

Solely because the posterior correction makes the CSAT3 more omnidirectional does not imply that field measurements of vertical wind and turbulent fluxes are impacted, nor does this assure that these impacts would be due to anything more than chance. Even with the uncertainty in the posterior w correction explicitly quantified (Fig. 7d) it is difficult to foresee if w is

Atmos. Meas. Tech. Discuss., doi:10.5194/amt-2016-145, 2016
Manuscript under review for journal Atmos. Meas. Tech.
Published: 23 June 2016

significantly impacted without applying the posterior correction to actual data. A powerful attribute of the Bayesian analysis is that the posterior correction can be applied to raw data to produce probability distribution estimates for w and H from which statistical inferences can be made. Using GLEES data, Fig. 11c-d confirms that to achieve an omnidirectional sensor (Fig. 10) with minimal change to horizontal winds (Fig. 11a-b) the required correction will increase both w and H by an average of 10.6% and 9.9%, which is significantly more (>95% credible interval) than predicted by the Kaimal prior. We argue that this significant increase in the vertical wind occurs because the posterior correction more accurately accounts for all shadowing between transducers (Fig. 9 versus Fig. 3), therefore we support our second hypothesis.

Also of note, there are instabilities in the prior and posterior w corrections for near-equatorial winds that occur at latitudes less than ±4° (6 inflection points around the equator, Fig. 3f and 9f). The mathematical cause for these instabilities and the locations of the inflection points are derived in Appendix A.2, and unless the corrections for the three transducers are exactly equal everywhere around the equator these instabilities will exist. The existence of these instabilities should cause concern for eddy-covariance measurements. The ultimate impact of this phenomena is difficult to know, because on one hand, w for latitudes less than ±4° are by definition very small, but on the other, these eddies constitute a large proportion of winds that exist under field conditions and their correction is currently unpredictable. For example, at GLEES 30% of winds occur at latitudes within ±4° (unpublished analysis of Figure 4 from Frank et al. (2016)). It is unknown how aggressively the correction for these winds approaches $\pm\infty$ or if more inflection points actually occur. For all non-orthogonal geometries, not just the CSAT3, if any transducer shadowing occurs at the equator, there will be instabilities in the w correction.

4.4 Impact across global flux networks

Atmos. Meas. Tech. Discuss., doi:10.5194/amt-2016-145, 2016
Manuscript under review for journal Atmos. Meas. Tech.
Published: 23 June 2016

Atmospheric Measurement Techniques Discussions

Energy balance is a fundamental ecosystem concept where the flow of available energy into an ecosystem influences the microclimate, drives photosynthesis, and establishes trophic levels among the biota (Odum, 1957; Fisher and Likens, 1973; Teal, 1962). Yet, eddy covariance studies of ecosystem fluxes seldom delve into details of energy flow beyond the generation of sensible and latent heat. It is often stated that most eddy covariance sites underestimate these turbulent components of the energy balance by 10-20% when compared to the available energy (Wilson et al., 2002; Foken, 2008; Stoy et al., 2013; Leuning et al., 2012; Franssen et al., 2010). Even when sites thoroughly account for lesser components such as energy stored in the biomass or canopy air, the turbulent energy can still be 1-14% underestimated (Heilman et al., 2009; Oliphant et al., 2004; Barr et al., 2006; Wang et al., 2012). It is common for sites to deal with this problem by forcing energy balance closure by increasing *H* and/or *LE* (Heilman et al., 2009; Oliphant et al., 2004; Twine et al., 2000; Scott et al., 2004) or even carbon fluxes (Barr et al., 2006) by the percent of the energy imbalance. Is there a mechanistic reason why so many sites believe their turbulent fluxes are underestimated? While it is difficult to generalize for every site, one similarity among these studies (Heilman et al., 2009; Oliphant et al., 2004; Barr et al., 2006; Wang et al., 2012; Twine et al., 2000; Scott et al., 2004) is they all feature a CSAT3, as do ~60% of all sites in the AmeriFlux network (unpublished summary of 150 the 228 sites where anemometer information was available, list accessed at http://ameriflux.lbl.gov/ in November 2015) and numerous sites distributed across the world within FLUXNET (http://fluxnet.fluxdata.org/).

After applying the posterior correction to the CSAT3 at our site, measurements of one of the energy balance components, *H*, increased 9.9 ± 1.6%, which is about twice the 5.5% increase predicted the Kaimal correction (Fig. 11) (note, the field experiments were conducted without a co-located fast-response hygrometer, hence we do not estimate the impact on *LE* at our site). However, we must consider that our field site in Wyoming is unusual, with extreme wind and turbulence, and where summer friction velocity (u_*) averages 0.6 m s^{-1} (Frank et al., 2016). While this made GLEES a good location to conduct the turbulent field experiments that led to the development of the posterior correction, do our results lead to similar impacts on ecosystem fluxes elsewhere? To answer this we applied the posterior correction to eddy covariance measurements at various sites across North America that employ the CSAT3 (Table 2). We found that the sum of the turbulent components of the energy balance (sensible plus latent heat flux) increased on average between 8-12% with the average 95% credible interval being 6-14%. At most sites this was significantly higher than applying the Kaimal correction. Thus, it is highly probable that at flux sites that employ the CSAT3 sonic anemometer the posterior correction will significantly increase the turbulent components of the energy budget and explain much of the ubiquitous energy imbalance problem; therefore we support our third hypothesis.

Are the results from this study applicable to the non-orthogonal sonic anemometers produced by other manufacturers? Possibly. Frank et al. (2016) showed that the Applied Technologies, Inc. A-probe shares a similar transducer geometry, a lack of a shadow correction algorithm, and similar differences between vertically and horizontally mounted anemometers, so it would be reasonable to expect a similar 3D correction for that instrument. But other manufacturers do apply wake corrections in their firmware that are traceable to wind tunnel calibrations. Are these adequate? Maybe not, as non-orthogonal anemometers from other manufacturers have been implicated to erroneously measure the vertical wind (Kochendorfer et al., 2012; Nakai et al., 2014; Nakai and Shimoyama, 2012). Without details of the calibrations or the wake corrections it is difficult to know. Regardless, for any non-orthogonal sonic

Atmos. Meas. Tech. Discuss., doi:10.5194/amt-2016-145, 2016
Manuscript under review for journal Atmos. Meas. Tech.
Published: 23 June 2016

Atmospheric Measurement Techniques Discussions

anemometer with vertically oriented transducers, equatorial instabilities are likely to exist (Appendix A.2) that would be extremely difficult to characterize with only a series of wind tunnel calibrations. One benefit of our methodology is that it allows an independent check on the sufficiency of these wake corrections. If such an instrument fails to consistently measure 3-dimensional winds (i.e., it responds like Fig. 2), then our methodology would estimate a posterior correction that could correct a wake-corrected anemometer. Because ~90% of all AmeriFlux sites use non-orthogonal sonic anemometers (Frank et al., 2013; Nakai et al., 2014), it would be appropriate to investigate this issue for all non-orthogonal sonic anemometer designs.

4.5 The next step

While these results reveal much about the nature of shadowing in a non-orthogonal sonic anemometer, there is much more to be done. First, due to the intense computational burden of this analysis we never fully utilized our data. While we only analyzed 5% of the available data, limited the 3D correction to approximately ±5° resolution and only 138 unique corrections, and terminated the Bayesian MCMC chains after only 10,000 steps, it still took months of continuous processing with extensive memory usage to produce these results. Obviously there is an opportunity to adapt this analysis to run on multiple cores or a supercomputer. As we developed our analysis it became apparent that with more data the standard deviations of the posterior distribution improved; we foresee that with 20 times more data the uncertainty in the posterior correction would be further reduced. Adaptation to a high-performance computer will allow for a more precise grid, longer MCMC chains, and a lower standard deviation of the posterior distribution.

Our results draw extensively on the symmetry of the CSAT3, which fails to account for the upper and lower mounting arms that extend back into the electronics housing and support

Atmos. Meas. Tech. Discuss., doi:10.5194/amt-2016-145, 2016
Manuscript under review for journal Atmos. Meas. Tech.
Published: 23 June 2016

block. We beta tested our model to solve for the 3D correction independently for each transducer and for all grid points around the sphere. We abandoned this because winds at GLEES are fairly unidirectional causing many of the grid points to be poorly characterized. Plus with an order of magnitude more unique grid points to solve, the computation took over 5 months to complete just one MCMC chain! There is a middle ground between assuming symmetry and pooling data, i.e., the correction for the A transducer pair could be considered symmetrical along the *u*-*w* plane and the corrections for transducer pairs B and C are mirror images of each other. In addition to solving the problem with less assumptions of symmetry, more experimental manipulations should be tested. We only tested a 90° rotation along the *u*-axis, but there are limitless other manipulations that would help characterize the shadowing around the entire 3D space surrounding an anemometer. Our model could easily be adapted to handle different manipulations using Eq. (7). This equation can be expanded to account for a limitless number of manipulations within the same analysis.

Our results using the posterior correction (Fig. 10) show that there is still unexplained residual error, though we expect some of this to be reduced with our suggestions above. While Horst et al. (2015) showed that to a first order that transducer shadowing is a function of the longitude and latitude of the instantaneous wind, the impact of other covariates such as wind velocity and turbulence may need to be considered. An advantage of performing our analysis in a Bayesian framework is that the model can be expanded to incorporate the effects of these covariates.

And finally, our posterior correction and methodology should be compared to other independent analysis of sonic anemometer shadowing such as wind tunnel data (Horst et al., 2015) or an independent Doppler Lidar system (Sathe et al., 2011). Care should be taken when

Atmos. Meas. Tech. Discuss., doi:10.5194/amt-2016-145, 2016
Manuscript under review for journal Atmos. Meas. Tech.
Published: 23 June 2016

incorporating these results, as anemometers could respond differently under laminar flow in a wind tunnel versus under turbulent field conditions. Regardless, a key to resolving this problem will be to embrace new technologies, new experimental designs, and new analyses.

5 Conclusion

The non-orthogonal CSAT3 sonic anemometer produces different results (Fig. 2) when it is mounted horizontally instead of vertically (Fig. 1). Assuming that the primary source of this error is shadowing across the various transducers, a Bayesian model can estimate a posterior correction (Fig. 8) that ultimately makes measurements from vertically and horizontally mounted anemometers most similar (Fig. 10). Even when taking into account the uncertainty of the posterior correction (Fig. 7) the increases in vertical wind velocity and sensible heat flux measurements are significantly larger and are approximately twice the magnitude of the Kaimal correction (Fig. 11). When this posterior correction is applied to various eddy covariance sites across North America, the turbulent components of the ecosystem energy balance (sensible plus latent heat flux) increased between 8.1-11.6%, with an average 95% confidence that this increase was between 6.1-13.8% (Table 2). Considering this is the most common sonic anemometer in the AmeriFlux network and is found in all the regional networks that comprise FLUXNET, these results have major implications for countless studies that use the eddy-covariance technique to measure terrestrial/atmospheric exchange of mass and energy.

Acknowledgments

We thank Jorge Ramirez, Susan Howe, Mario Bretfeld, Kelly Elder, Banning Starr, Bill Kustas, and Joe Alfieri for providing data from their unique field sites. We especially thank Ben

Atmos. Meas. Tech. Discuss., doi:10.5194/amt-2016-145, 2016
Manuscript under review for journal Atmos. Meas. Tech.
Published: 23 June 2016

Atmospheric Measurement Techniques Discussions
Open Access

Bird for his countless hours of statistical advice in developing the Bayesian model. This study was funded by the U.S. Forest Service, the Wyoming Water Development Commission, the USGS, the NSF (awards EPS-1208909 and EAR-0444053), and the DOD Army Research Office (W911NF-05-1-0558 and W911NF-05-1-0126).

Appendix

A.1 Univariate conditional posterior distribution functions for Gibbs sampling

For the univariate conditional posterior distribution functions there is a distinction between independent grid points versus those linked together through symmetry. In the case of the former, these functions can be evaluated for each unique grid point, *g*, for each transducer pair, *t*. In the case of the latter, *g* and *t* refer to the sets of all grid points and transducers that share the same unique state variable for their shadow correction, and these functions can be applied to each of these unique sets.

First, using Bayes Theorem, the joint posterior distribution of the model parameters can be expressed as being proportional to the product of the likelihood of the data and the joint prior distribution of the model parameters (Eq. A1).

$$p\left(\tilde{\sigma}_{F\times C_{f,c}}, \alpha_{T\times G_{t,g}}, \varepsilon \middle| \sigma_{f,i,c}\right) \propto p\left(\sigma_{f,i,c} \middle| \tilde{\sigma}_{F\times C_{f,c}}, \alpha_{T\times G_{t,g}}, \varepsilon\right) p\left(\tilde{\sigma}_{F\times C_{f,c}}, \alpha_{T\times G_{t,g}}, \varepsilon\right) \quad \text{(A1)}$$

Because the prior distributions for three model parameters are independent, the joint prior distribution can be written as the product of the individual probabilities (Eq. A2).

$$p\left(\tilde{\sigma}_{F\times C_{f,c}}, \alpha_{T\times G_{t,g}}, \varepsilon \middle| \sigma_{f,i,c}\right) \propto p\left(\sigma_{f,i,c} \middle| \tilde{\sigma}_{F\times C_{f,c}}, \alpha_{T\times G_{t,g}}, \varepsilon\right) p\left(\tilde{\sigma}_{F\times C_{f,c}}\right) p\left(\alpha_{T\times G_{t,g}}\right) p(\varepsilon)$$

(A2)

The likelihood of the data is normally distributed (Eq. A3).

$$p\left(\sigma_{f,i,c} \middle| \tilde{\sigma}_{F\times C_{f,c}}, \alpha_{T\times G_{t,g}}, \varepsilon\right) = \frac{1}{\sqrt{2\pi}\varepsilon} e^{\left(-\frac{1}{2\varepsilon^2}\left(\sigma_{f,i,c} - \hat{\sigma}_{f,i,c}\right)^2\right)} \quad \text{(A3)}$$

Atmos. Meas. Tech. Discuss., doi:10.5194/amt-2016-145, 2016
Manuscript under review for journal Atmos. Meas. Tech.
Published: 23 June 2016

Atmospheric Measurement Techniques Discussions
Open Access

Because $\hat{\sigma}_{f,i,c}$ is both a function of $\tilde{\sigma}_{F\times C_{f,c}}$ and $\alpha_{T\times G_{t,g}}$ the likelihood is indeed a function of all three model parameters. The individual prior distributions for $\tilde{\sigma}_{F\times C_{f,c}}$, $\alpha_{T\times G_{t,g}}$, and ε are uniformly (Eq. A4), normally (Eq. A5), and gamma (Eq. A6) distributed, respectively.

$$p\left(\tilde{\sigma}_{F\times C_{f,c}}\right) = \begin{cases} \frac{1}{max(U_C)}, & 0 \leq \tilde{\sigma}_{F\times C_{f,c}} \leq max(U_C) \\ 0, & otherwise \end{cases} \tag{A4}$$

$$p\left(\alpha_{T\times G_{t,g}}\right) = \frac{1}{\sqrt{2\pi}(0.1)} e^{\left(-\frac{1}{2(0.1)^2}\left(\alpha_{T\times G_{t,g}} - P_{t,g}\right)^2\right)} \tag{A5}$$

$$p(\varepsilon) = \acute{b}e^{-\acute{b}} \tag{A6}$$

Gibbs sampling for each model parameter is based on the univariate conditional posterior distribution which assumes that all other model parameters plus the data are given (in the case of sampling within a multidimensional array, all other parameters within that array are given except the one at the index being evaluated). For $\tilde{\sigma}_{F\times C_{f,c}}$ the univariate conditional posterior distribution can be expressed as a form of Bayes Theorem (Eq. A7).

$$p\left(\tilde{\sigma}_{F\times C_{f,c}} \middle| \underline{\tilde{\sigma}_{F\times C}}_{-f,c}, \underline{\alpha_{T\times G}}, \varepsilon, \underline{\sigma}\right) = \frac{p\left(\underline{\tilde{\sigma}_{F\times C}}, \underline{\alpha_{T\times G}}, \varepsilon \middle| \underline{\sigma}\right) p(\underline{\sigma})}{p\left(\underline{\tilde{\sigma}_{F\times C}}_{-f,c}, \underline{\alpha_{T\times G}}, \varepsilon, \underline{\sigma}\right)} \tag{A7}$$

The under-bar denotes all elements within a multidimensional array, while the notation $\underline{\tilde{\sigma}_{F\times C}}_{-f,c}$ means all elements of $\vec{\tilde{\sigma}}_{F\times C}$ except for $\tilde{\sigma}_{F\times C_{f,c}}$. On right side of Eq. A7, both the second term in the numerator and the denominator are assumed given and can be omitted if the equal sign is changed to a proportional sign. The first term in the numerator, $p\left(\underline{\tilde{\sigma}_{F\times C}}, \underline{\alpha_{T\times G}}, \varepsilon \middle| \underline{\sigma}\right)$, is the joint posterior distribution summed across all parameters (Eq. A8).

$$p\left(\underline{\tilde{\sigma}_{F\times C}}, \underline{\alpha_{T\times G}}, \varepsilon \middle| \underline{\sigma}\right) \propto$$

$$\prod_{f=1}^{F}\prod_{c=1}^{3}\left\{\left[\prod_{i=1}^{I} p\left(\sigma_{f,i,c} \middle| \tilde{\sigma}_{F\times C_{f,c}}, \alpha_{T\times G_{t,g}}, \varepsilon\right)\right] p\left(\tilde{\sigma}_{F\times C_{f,c}}\right)\right\} \prod_{t=1}^{3}\prod_{g=1}^{G} p\left(\alpha_{T\times G_{t,g}}\right) p(\varepsilon) \tag{A8}$$

Atmos. Meas. Tech. Discuss., doi:10.5194/amt-2016-145, 2016
Manuscript under review for journal Atmos. Meas. Tech.
Published: 23 June 2016

Atmospheric Measurement Techniques
Discussions

Assuming that all but $\tilde{\sigma}_{F\times C_{f,c}}$ is given plus requiring that the proposed value for $\tilde{\sigma}_{F\times C_{f,c}}$ is within the valid range (i.e., $p\left(\tilde{\sigma}_{F\times C_{f,c}}\right)$ is constant and can be omitted) Eq. A7 simplifies to Eq. A9.

$$p\left(\tilde{\sigma}_{F\times C_{f,c}} \middle| \underline{\tilde{\sigma}_{F\times C}}_{-f,c}, \underline{\alpha_{T\times G}}, \varepsilon, \underline{\sigma}\right) \propto \prod_{i=1}^{I} p\left(\sigma_{f,i,c} \middle| \tilde{\sigma}_{F\times C_{f,c}}, \alpha_{T\times G_{t,g}}, \varepsilon\right) \quad \text{(A9)}$$

Substituting in the likelihood from Eq. A3 and simplifying gives the univariate conditional posterior distribution for $\tilde{\sigma}_{F\times C_{f,c}}$ (Eq. A10).

$$p\left(\tilde{\sigma}_{F\times C_{f,c}} \middle| \underline{\tilde{\sigma}_{F\times C}}_{-f,c}, \underline{\alpha_{T\times G}}, \varepsilon, \underline{\sigma}\right) \propto e^{\left(-\frac{1}{2\varepsilon^2}\sum_{i=1}^{I}\left(\sigma_{f,i,c}-\hat{\sigma}_{f,i,c}\right)^2\right)} \quad \text{(A10)}$$

The univariate conditional posterior distribution for $\alpha_{T\times G_{t,g}}$ can be expressed as Bayes Theorem (Eq. A11).

$$p\left(\alpha_{T\times G_{t,g}} \middle| \underline{\tilde{\sigma}_{F\times C}}, \underline{\alpha_{T\times G}}_{-t,g}, \varepsilon, \underline{\sigma}\right) = \frac{p\left(\underline{\tilde{\sigma}_{F\times C}}, \underline{\alpha_{T\times G}}, \varepsilon \middle| \underline{\sigma}\right) p\left(\underline{\sigma}\right)}{p\left(\underline{\tilde{\sigma}_{F\times C}}, \underline{\alpha_{T\times G}}_{-t,g}, \varepsilon, \underline{\sigma}\right)} \quad \text{(A11)}$$

Again, only the first term in the numerator must be evaluated while assuming that all but $\alpha_{T\times G_{t,g}}$ are given (Eq. A12).

$$p\left(\alpha_{T\times G_{t,g}} \middle| \underline{\tilde{\sigma}_{F\times C}}, \underline{\alpha_{T\times G}}_{-t,g}, \varepsilon, \underline{\sigma}\right) \propto \prod_{f=1}^{F}\prod_{i=1}^{I}\prod_{c=1}^{3} p\left(\sigma_{f,i,c} \middle| \tilde{\sigma}_{F\times C_{f,c}}, \alpha_{T\times G_{t,g}}, \varepsilon\right) p\left(\alpha_{T\times G_{t,g}}\right)$$

(A12)

Substituting in both the likelihood of the data (Eq. A3) and the prior distribution for $\alpha_{T\times G_{t,g}}$ (Eq. A5) and simplifying yields the univariate conditional posterior distribution for $\alpha_{T\times G_{t,g}}$ (Eq. A13).

$$p\left(\alpha_{T\times G_{t,g}} \middle| \underline{\tilde{\sigma}_{F\times C}}, \underline{\alpha_{T\times G}}_{-t,g}, \varepsilon, \underline{\sigma}\right) \propto e^{\left(-\frac{1}{2\varepsilon^2}\sum_{f=1}^{F}\sum_{i=1}^{I}\sum_{c=1}^{3}\left(\sigma_{f,i,c}-\hat{\sigma}_{f,i,c}\right)^2-\frac{1}{2(0.1)^2}\left(\alpha_{T\times G_{t,g}}-P_{t,g}\right)^2\right)}$$

(A13)

An important issue is that $\hat{\sigma}_{f,i,c}$ is a function of $\alpha_{T\times G_{t,g}}$ and must be evaluated for every proposed change to the 3D correction. This is computationally intensive and causes a bottleneck in the analysis. Finally, the univariate conditional posterior distribution for ε can be expressed as Bayes Theorem (Eq. A14).

$$p\left(\varepsilon\middle|\underline{\tilde{\sigma}_{F\times C}},\underline{\alpha_{T\times G}},\underline{\sigma}\right)=\frac{p\left(\underline{\tilde{\sigma}_{F\times C}},\underline{\alpha_{T\times G}},\varepsilon\middle|\underline{\sigma}\right)p(\underline{\sigma})}{p\left(\underline{\tilde{\sigma}_{F\times C}},\underline{\alpha_{T\times G}},\underline{\sigma}\right)} \quad \text{(A14)}$$

Only the first term in the numerator must be evaluated while assuming that all but ε are given (Eq. A15).

$$p\left(\varepsilon\middle|\underline{\tilde{\sigma}_{F\times C}},\underline{\alpha_{T\times G}},\underline{\sigma}\right)\propto\prod_{f=1}^{F}\prod_{i=1}^{I}\prod_{c=1}^{3}p\left(\sigma_{f,i,c}\middle|\tilde{\sigma}_{F\times C_{f,c}},\alpha_{T\times G_{t,g}},\varepsilon\right) \quad \text{(A15)}$$

Substituting in the likelihood from Eq. A3 and simplifying yields the univariate conditional posterior distribution for ε (Eq. A16)

$$p\left(\varepsilon\middle|\underline{\tilde{\sigma}_{F\times C}},\underline{\alpha_{T\times G}},\underline{\sigma}\right)\propto\varepsilon^{-3FI}e^{\left(-\frac{1}{2\varepsilon^2}\sum_{f=1}^{F}\sum_{c=1}^{3}\sum_{i=1}^{I}\left(\sigma_{f,i,c}-\hat{\sigma}_{f,i,c}\right)^2\right)} \quad \text{(A16)}$$

A.2 Instability in the *w* correction for near equatorial winds

For a CSAT3, the amount of correction applied to the vertical wind velocity, expressed as the individual corrections $\alpha_A(\lambda,\varphi)$, $\alpha_B(\lambda,\varphi)$, and $\alpha_C(\lambda,\varphi)$ for the three transducer pairs *A*, *B*, and *C* as functions of longitude, λ, and latitude, φ, is:

$$\frac{w_{corrected}}{w_{uncorrected}}=\frac{2}{3\sqrt{3}}\left[\left(-\frac{\cos\lambda}{2\tan\varphi}+\frac{\sqrt{3}}{2}\right)\alpha_A(\lambda,\varphi)+\left(\frac{\cos\lambda+\sqrt{3}\sin\lambda}{4\tan\varphi}+\frac{\sqrt{3}}{2}\right)\alpha_B(\lambda,\varphi)+\left(\frac{\cos\lambda-\sqrt{3}\sin\lambda}{4\tan\varphi}+\frac{\sqrt{3}}{2}\right)\alpha_C(\lambda,\varphi)\right] \quad \text{(A17)}$$

If the individual corrections for the three transducer pairs never approach 0 or $\pm\infty$, which is a safe assumption considering they are always around 1 (Figs. 3a, c, e and 9a, c, e), the limit of this as the latitude approaches the equator is:

$$\lim_{\varphi\to 0}\frac{w_{corrected}}{w_{uncorrected}} = \frac{1}{3}\left(\alpha_A(\lambda,\varphi)+\alpha_B(\lambda,\varphi)+\alpha_C(\lambda,\varphi)\right)+$$

$$\frac{2}{3\sqrt{3}}\left[\left(-\frac{\cos\lambda}{2}\right)\alpha_A(\lambda,\varphi)+\left(\frac{\cos\lambda+\sqrt{3}\sin\lambda}{4}\right)\alpha_B(\lambda,\varphi)+\left(\frac{\cos\lambda-\sqrt{3}\sin\lambda}{4}\right)\alpha_C(\lambda,\varphi)\right]\lim_{\varphi\to 0}\frac{1}{\tan\varphi} \quad \text{(A18)}$$

This approaches $\pm\infty$ unless the terms associated with the limit of the tangent exactly cancel. This is achieved if $\alpha_A(\lambda,0°)=\alpha_B(\lambda,0°)=\alpha_C(\lambda,0°)$, which includes the special case where $\alpha_A(\lambda,0°)=\alpha_B(\lambda,0°)=\alpha_C(\lambda,0°)=1$. Based on our assumptions of symmetry with the CSAT3, $\alpha_B(\lambda,\varphi)=\alpha_A(60°-\lambda,-\varphi)$ and $\alpha_C(\lambda,\varphi)=\alpha_A(60°+\lambda,-\varphi)$. Therefore, the w correction for near equatorial winds is unstable unless:

$$\alpha_A(\lambda,0°)=\frac{1+\sqrt{3}\tan\lambda}{2}\alpha_A(60°-\lambda,0°)+\frac{1-\sqrt{3}\tan\lambda}{2}\alpha_A(60°+\lambda,0°) \quad \text{(A19)}$$

This is satisfied by λ = 30°, 90°, 150°, 210°, 270°, and 330°. Eq. A19 shows that if the weighted average of $\alpha_A(60°-\lambda,-\varphi)$ and $\alpha_A(60°+\lambda,-\varphi)$ cancel $\alpha_A(\lambda,0°)$ then the correction will be stable. This cannot be achieved if the correction $\alpha_A(\lambda,0°)$ is monotonic between 0° ≤ λ ≤ 90°. Because the w correction is symmetric every 30°, any solution besides λ = 30°, 90°, 150°, 210°, 270°, and 330° will be mirrored 12 times.

Atmos. Meas. Tech. Discuss., doi:10.5194/amt-2016-145, 2016
Manuscript under review for journal Atmos. Meas. Tech.
Published: 23 June 2016

Atmospheric Measurement Techniques
Discussions

References

Anderson, R. G., and Wang, D.: Energy budget closure observed in paired eddy covariance towers with increased and continuous daily turbulence, Agricultural and Forest Meteorology, 184, 204-209, doi: 10.1016/j.agrformet.2013.09.012, 2014.

Baldocchi, D. D.: Assessing the eddy covariance technique for evaluating carbon dioxide exchange rates of ecosystems: past, present and future, Glob. Change Biol., 9, 479-492, doi: 10.1046/j.1365-2486.2003.00629.x, 2003.

Barr, A. G., Morgenstern, K., Black, T. A., McCaughey, J. H., and Nesic, Z.: Surface energy balance closure by the eddy-covariance method above three boreal forest stands and implications for the measurement of the CO_2 flux, Agricultural and Forest Meteorology, 140, 322-337, doi: 10.1016/j.agrformet.2006.08.007, 2006.

Barrett, E. W., and Suomi, V. E.: Preliminary report on temperature measurement by sonic means, Journal of Meteorology, 6, 273-276, doi: doi:10.1175/1520-0469(1949)006<0273:PROTMB>2.0.CO;2, 1949.

Bayes, M., and Price, M.: An Essay towards solving a problem in the doctrine of chances. By the Late Rev. Mr. Bayes, F. R. S. Communicated by Mr. Price, in a letter to John Canton, A. M. F. R. S, Philosophical Transactions, 53, 370-418, doi: 10.1098/rstl.1763.0053, 1763.

Biederman, J. A., Harpold, A. A., Gochis, D. J., Ewers, B. E., Reed, D. E., Papuga, S. A., and Brooks, P. D.: Increased evaporation following widespread tree mortality limits streamflow response, Water Resour. Res., 50, 5395-5409, doi: 10.1002/2013wr014994, 2014.

Buks, E., Schuster, R., Heiblum, M., Mahalu, D., and Umansky, V.: Dephasing in electron interference by a 'which-path' detector, Nature, 391, 871-874, doi, 1998.

Dellwik, E., Sjöholm, M., and Mann, J.: An evaluation of the WindEye wind lidar, DTU Wind Energy, Report, 2015.

Fisher, S. G., and Likens, G. E.: Energy flow in Bear Brook, New Hampshire: An integrative approach to stream ecosystem metabolism, Ecological Monographs, 43, 421-439, doi: 10.2307/1942301, 1973.

Foken, T.: The energy balance closure problem: An overview, Ecol. Appl., 18, 1351-1367, doi: 10.1890/06-0922.1, 2008.

Frank, J. M., Massman, W. J., and Ewers, B. E.: Underestimates of sensible heat flux due to vertical velocity measurement errors in non-orthogonal sonic anemometers, Agricultural and Forest Meteorology, 171–172, 72-81, doi: 10.1016/j.agrformet.2012.11.005, 2013.

Frank, J. M., Massman, W. J., Ewers, B. E., Huckaby, L. S., and Negrón, J. F.: Ecosystem CO_2/H_2O fluxes are explained by hydraulically limited gas exchange during tree mortality from spruce bark beetles, Journal of Geophysical Research: Biogeosciences, 119, 1195-1215, doi: 10.1002/2013jg002597, 2014.

Frank, J. M., Massman, W. J., Swiatek, E., Zimmerman, H. A., and Ewers, B. E.: All sonic anemometers need to correct for transducer and structural shadowing in their velocity measurements, J. Atmos. Ocean. Technol., 33, 149-167, doi: 10.1175/jtech-d-15-0171.1, 2016.

Franssen, H. J. H., Stockli, R., Lehner, I., Rotenberg, E., and Seneviratne, S. I.: Energy balance closure of eddy-covariance data: A multisite analysis for European FLUXNET stations, Agricultural and Forest Meteorology, 150, 1553-1567, doi: 10.1016/j.agrformet.2010.08.005, 2010.

Atmos. Meas. Tech. Discuss., doi:10.5194/amt-2016-145, 2016
Manuscript under review for journal Atmos. Meas. Tech.
Published: 23 June 2016

Friebel, H. C., Herrington, T. O., and Benilov, A. Y.: Evaluation of the flow distortion around the Campbell Scientific CSAT3 sonic anemometer relative to incident wind direction, J. Atmos. Ocean. Technol., 26, 582-592, doi: 10.1175/2008jtecho550.1, 2009.

Gelman, A., Carlin, J. B., Stern, H. S., and Rubin, D. B.: Bayesian Data Analysis, 2nd ed., Chapman & Hall/CRC Press, Boca Raton, FL, 668 pp., 2004.

Heilman, J. L., McInnes, K. J., Kjelgaard, J. F., Keith Owens, M., and Schwinning, S.: Energy balance and water use in a subtropical karst woodland on the Edwards Plateau, Texas, Journal of Hydrology, 373, 426-435, doi: http://dx.doi.org/10.1016/j.jhydrol.2009.05.007, 2009.

Hogstrom, U., and Smedman, A. S.: Accuracy of sonic anemometers: Laminar wind-tunnel calibrations compared to atmospheric in situ calibrations against a reference instrument, Bound.-Layer Meteor., 111, 33-54, doi: 10.1023/b:boun.0000011000.05248.47, 2004.

Horst, T. W., Semmer, S. R., and Maclean, G.: Correction of a non-orthogonal, three-component sonic anemometer for flow distortion by transducer shadowing, Bound.-Layer Meteor., 1-25, doi: 10.1007/s10546-015-0010-3, 2015.

Kaimal, J. C., and Businger, J. A.: A continuous wave sonic anemometer-thermometer, Journal of Applied Meteorology, 2, 156-164, doi: 10.1175/1520-0450(1963)002<0156:acwsat>2.0.co;2, 1963.

Kaimal, J. C.: Sonic anemometer measurement of atmospheric turbulence, Proceedings of the Dynamic Flow Conference 1978 on Dynamic Measurements in Unsteady Flows, Skovlunde, Denmark, 1979, 551-565,

Kochendorfer, J., Meyers, T. P., Frank, J. M., Massman, W. J., and Heuer, M. W.: How well can we measure the vertical wind speed? Implications for fluxes of energy and mass, Bound.-Layer Meteor., 145, 383-398, doi: 10.1007/s10546-012-9738-1, 2012.

Kruschke, J.: Doing Bayesian data analysis: A tutorial introduction with R and BUGS, Academic Press, 2010.

Lee, X., Finnigan, J. J., and Paw U, K. T.: Coordinate system and flux bias error, in: Handbook of micrometeorology, edited by: Lee, X., Massman, W. J., and Law, B. E., Kluwer Academic Publishers, Dordrecht, The Netherlands, 33-66, 2004.

Leuning, R., van Gorsel, E., Massman, W. J., and Isaac, P. R.: Reflections on the surface energy imbalance problem, Agricultural and Forest Meteorology, 156, 65-74, doi: 10.1016/j.agrformet.2011.12.002, 2012.

Lu, Y., Ye, K., Mathur, A. K., Hui, S., Fuerst, T. P., and Genant, H. K.: Comparative calibration without a gold standard, Statistics in Medicine, 16, 1889-1905, doi: 10.1002/(sici)1097-0258(19970830)16:16<1889::aid-sim607>3.0.co;2-v, 1997.

MacLean, W. R.: Absolute Measurement of Sound Without a Primary Standard, The Journal of the Acoustical Society of America, 12, 140-146, doi: doi:http://dx.doi.org/10.1121/1.1916085, 1940.

Massman, W. J., and Lee, X.: Eddy covariance flux corrections and uncertainties in long-term studies of carbon and energy exchanges, Agricultural and Forest Meteorology, 113, 121-144, doi: 10.1016/s0168-1923(02)00105-3, 2002.

Monnier, T., Seydou, D., Godin, N., and Zhang, F.: Primary calibration of acoustic emission sensors by the method of reciprocity, theoretical and experimental considerations, Journal of Acoustic Emission, 30, 152-166, doi, 2012.

Nakai, T., and Shimoyama, K.: Ultrasonic anemometer angle of attack errors under turbulent conditions, Agricultural and Forest Meteorology, 162–163, 14-26, doi: 10.1016/j.agrformet.2012.04.004, 2012.

Nakai, T., Iwata, H., Harazono, Y., and Ueyama, M.: An inter-comparison between Gill and Campbell sonic anemometers, Agricultural and Forest Meteorology, 195–196, 123-131, doi: 10.1016/j.agrformet.2014.05.005, 2014.

Odum, H. T.: Trophic structure and productivity of Silver Springs, Florida, Ecological Monographs, 27, 55-112, doi: 10.2307/1948571, 1957.

Oliphant, A. J., Grimmond, C. S. B., Zutter, H. N., Schmid, H. P., Su, H. B., Scott, S. L., Offerle, B., Randolph, J. C., and Ehman, J.: Heat storage and energy balance fluxes for a temperate deciduous forest, Agricultural and Forest Meteorology, 126, 185-201, doi: http://dx.doi.org/10.1016/j.agrformet.2004.07.003, 2004.

R Core Team: R: A language and environment for statistical computing, 2015,

Reba, M. L., Pomeroy, J., Marks, D., and Link, T. E.: Estimating surface sublimation losses from snowpacks in a mountain catchment using eddy covariance and turbulent transfer calculations, Hydrol. Process., 26, 3699-3711, doi: 10.1002/hyp.8372, 2012.

RStudio Team: RStudio: Integrated Development for R, 2015,

Sathe, A., Mann, J., Gottschall, J., and Courtney, M. S.: Can wind Lidars measure turbulence?, J. Atmos. Ocean. Technol., 28, 853-868, doi: 10.1175/jtech-d-10-05004.1, 2011.

Scott, R. L., Edwards, E. A., Shuttleworth, W. J., Huxman, T. E., Watts, C., and Goodrich, D. C.: Interannual and seasonal variation in fluxes of water and carbon dioxide from a riparian woodland ecosystem, Agricultural and Forest Meteorology, 122, 65-84, doi: http://dx.doi.org/10.1016/j.agrformet.2003.09.001, 2004.

Stoy, P. C., Mauder, M., Foken, T., Marcolla, B., Boegh, E., Ibrom, A., Arain, M. A., Arneth, A., Aurela, M., Bernhofer, C., Cescatti, A., Dellwik, E., Duce, P., Gianelle, D., van Gorsel, E., Kiely, G., Knohl, A., Margolis, H., McCaughey, H., Merbold, L., Montagnani, L., Papale, D., Reichstein, M., Saunders, M., Serrano-Ortiz, P., Sottocornola, M., Spano, D., Vaccari, F., and Varlagin, A.: A data-driven analysis of energy balance closure across FLUXNET research sites: The role of landscape scale heterogeneity, Agricultural and Forest Meteorology, 171–172, 137-152, doi: http://dx.doi.org/10.1016/j.agrformet.2012.11.004, 2013.

Teal, J. M.: Energy flow in the salt marsh ecosystem of Georgia, Ecology, 43, 614-624, doi: 10.2307/1933451, 1962.

Twine, T. E., Kustas, W. P., Norman, J. M., Cook, D. R., Houser, P. R., Meyers, T. P., Prueger, J. H., Starks, P. J., and Wesely, M. L.: Correcting eddy-covariance flux underestimates over a grassland, Agricultural and Forest Meteorology, 103, 279-300, doi: 10.1016/s0168-1923(00)00123-4, 2000.

van der Molen, M. K., Gash, J. H. C., and Elbers, J. A.: Sonic anemometer (co)sine response and flux measurement - II. The effect of introducing an angle of attack dependent calibration, Agricultural and Forest Meteorology, 122, 95-109, doi: 10.1016/j.agrformet.2003.09.003, 2004.

Wahba, G.: Spline interpolation and smoothing on the sphere, SIAM Journal on Scientific and Statistical Computing, 2, 5-16, doi: doi:10.1137/0902002, 1981.

Wang, R., Zhang, Q., Zhao, H., Wang, H., and Wang, C.: Analysis of the surface energy closure for a site in the Gobi Desert in Northwest China, Acta Meteorologica Sinica, 26, 250-259, doi: 10.1007/s13351-012-0210-4, 2012.

Atmos. Meas. Tech. Discuss., doi:10.5194/amt-2016-145, 2016
Manuscript under review for journal Atmos. Meas. Tech.
Published: 23 June 2016

Atmospheric Measurement Techniques Discussions

Webb, E. K., Pearman, G. I., and Leuning, R.: Correction of flux measurements for density effects due to heat and water vapour transfer, Q. J. R. Meteorol. Soc., 106, 85-100, doi: 10.1256/smsqj.44706, 1980.

Welch, C. M., Stoy, P. C., Rains, F. A., Johnson, A. V., and McGlynn, B. L.: The impacts of mountain pine beetle disturbance on the energy balance of snow during the melt period, Hydrol. Process., n/a-n/a, doi: 10.1002/hyp.10638, 2015.

Wilson, K., Goldstein, A., Falge, E., Aubinet, M., Baldocchi, D., Berbigier, P., Bernhofer, C., Ceulemans, R., Dolman, H., Field, C., Grelle, A., Ibrom, A., Law, B. E., Kowalski, A., Meyers, T., Moncrieff, J., Monson, R., Oechel, W., Tenhunen, J., Valentini, R., and Verma, S.: Energy balance closure at FLUXNET sites, Agricultural and Forest Meteorology, 113, 223-243, doi: 10.1016/s0168-1923(02)00109-0, 2002.

Wood, S. N.: Generalized additive models: an introduction with R, Chapman and Hall/CRC, 2006.

Wyngaard, J. C., and Zhang, S.-F.: Transducer-shadow effects on turbulence spectra measured by sonic anemometers, J. Atmos. Ocean. Technol., 2, 548-558, doi: 10.1175/1520-0426(1985)002<0548:tseots>2.0.co;2, 1985.

Yahaya, S., and Frangi, J. P.: Cup anemometer response to the wind turbulence-measurement of the horizontal wind variance, Ann. Geophys., 22, 3363-3374, doi: 10.5194/angeo-22-3363-2004, 2004.

Atmos. Meas. Tech. Discuss., doi:10.5194/amt-2016-145, 2016
Manuscript under review for journal Atmos. Meas. Tech.
Published: 23 June 2016

Table 1. Summary of the subset of data from Frank et al. (2013) and Frank et al. (2016) reanalyzed in this study listing the four CSAT3 anemometers (A-D), their location within the five-position horizontal array, and if mounted horizontally (*). Because processing the Bayesian model is extremely intensive, only 5% of the available data was reanalyzed.

	Position					Number of 5-min periods	
Dates	1	2	3	4	5	Available	Reanalyzed
5-19 July 2011	A*	B	-	C	D*	2,520	126
19-26 July 2011	A	B*	-	C*	D	1,992	100
9-16 August 2011	B*	A	-	D	C*	1,974	98
16-22 August 2011	B	A*	-	D*	C	1,620	81
26-30 July 2013	A*	-	B	-	-	906	46
23-27 August 2013	-	-	A	-	B*	1,050	52
6-24 September 2013	-	-	B	D*	-	498	25

Atmos. Meas. Tech. Discuss., doi:10.5194/amt-2016-145, 2016
Manuscript under review for journal Atmos. Meas. Tech.
Published: 23 June 2016

Atmospheric Measurement Techniques
Discussions

Table 2. Increase in *H* + *LE* (sum of the turbulent components of the energy balance, i.e. sensible and latent heat flux) at various sites across North America after applying shadow correction to the CSAT3 time series data.

Site	Coordinates	Dates	Height (m)	Percent change after applying shadow correction: Kaimal correction	Percent change after applying shadow correction: Posterior correction mean ± standard deviation [95% credible interval]
Yuma, AZ, USA	33° 5' N 114° 32' W	6-15 June 2008	8.25	5.1%	9.8 ± 2.3% [5.1% 14.8%]
Yuma, AZ, USA	33° 5' N 114° 32' W	5-14 June 2009	2.00	4.5%	9.4 ± 2.8% [3.1% 16.1%]
Fraser, CO, USA	39° 53' 48.23" N 105° 53' 33.87" W	5-14 April 2015	27.50	5.6%	9.9 ± 1.4% [7.4% 12.2%]
Fraser, CO, USA	39° 53' 48.23" N 105° 53' 33.87" W	5-14 April 2015	6.40	6.8%	11.6 ± 1.2% [9.4% 13.9%]
Beltsville, MD, USA	39° 1' 51.23" N 76° 50' 39.40" W	16-31 July 2014	4.00	5.5%	10.4 ± 2.1% [6.3% 14.8%]
Glacier Peak, WY, USA	41° 22' 52" N 106° 15' 47" W	28 August-8 September 2015	3.20	5.3%	11.3 ± 3.1% [4.6% 19.2%]
Agua Salud, Panama	9° 13' 31.65" N 79° 45' 36.41" W	6-16 November 2015	5.00	4.7%	8.1 ± 1.6% [5.3% 10.8%]

Atmos. Meas. Tech. Discuss., doi:10.5194/amt-2016-145, 2016
Manuscript under review for journal Atmos. Meas. Tech.
Published: 23 June 2016

Atmospheric Measurement Techniques Discussions
Open Access

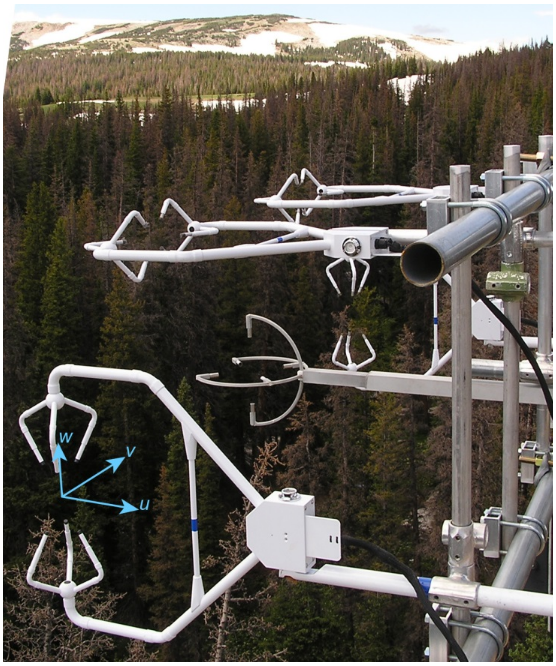

Fig. 1. Photograph of the 2011 experiment with two CSAT3 sonic anemometers mounted vertically and two horizontally. The cardinal *u*, *v*, and *w* axes are shown in light blue near one of the vertical instruments. Figure from Frank et al. (2013).

Atmos. Meas. Tech. Discuss., doi:10.5194/amt-2016-145, 2016
Manuscript under review for journal Atmos. Meas. Tech.
Published: 23 June 2016

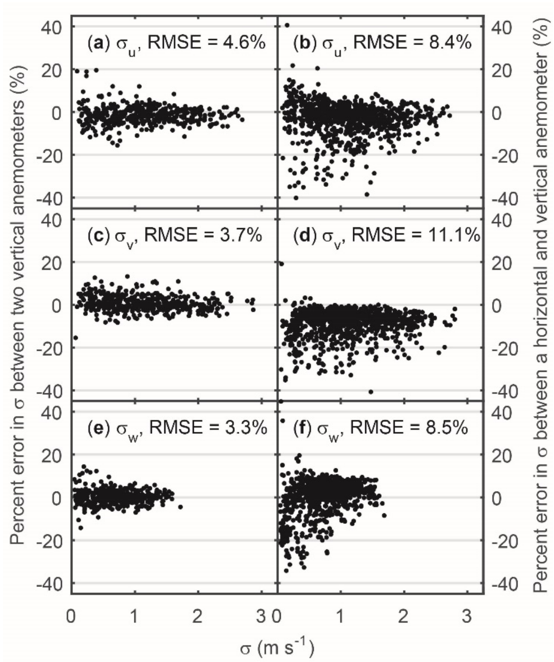

Fig. 2. Uncorrected measurements of the 5-minute standard deviation of wind (σ) along the cardinal (**a, b**) *u*, (**c, d**) *v*, and (**e, f**) *w* axes are not equivalent between vertically and horizontally mounted CSAT3 sonic anemometers. Data from an ideal 3D anemometer would have similar percent errors between a horizontal and a vertical anemometer (**b**, **d**, **f**) as found between two anemometers mounted vertically (**a**, **c**, **e**). The data are from 2011 and 2013 field experiments at the GLEES AmeriFlux site (Frank et al., 2016; Frank et al., 2013). The 2011 data in panels **b**, **d**, and **f** are randomly paired between the two anemometers in different orientations. Results are summarized as root mean square error (RMSE).

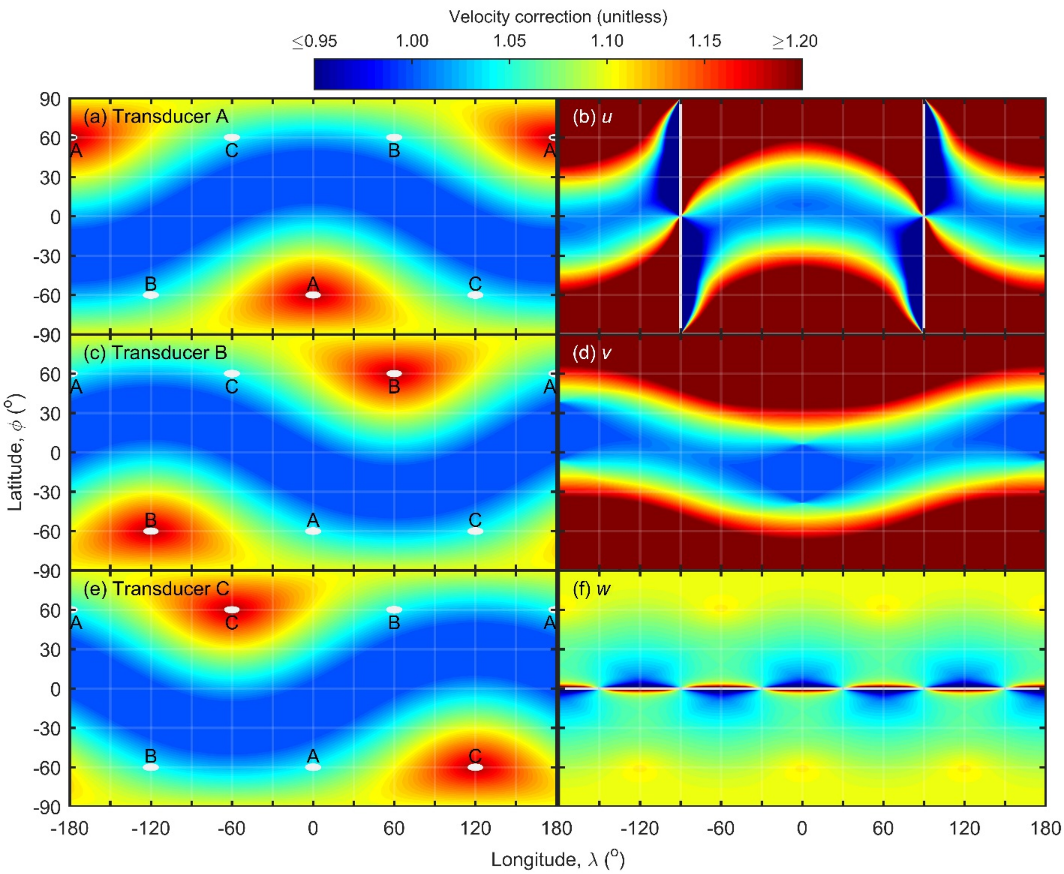

Fig. 3. The Kaimal correction, one of three priors tested in this study, for the (**a**) A, (**c**) B, and (**e**) C transducer pairs, each represented by a white dot, of a CSAT3 sonic anemometer accounts for self-shadowing but not cross-shadowing between transducers. The same correction expressed in sonic anemometer coordinates (**b**) *u*, (**d**) *v*, and (**f**) *w* shows that for near-equatorial winds, minimal correction is required for the horizontal wind components while significant correction and instability exist in the vertical wind component *w*. Longitude and latitude are relative to the *u* axis (Fig. 1).

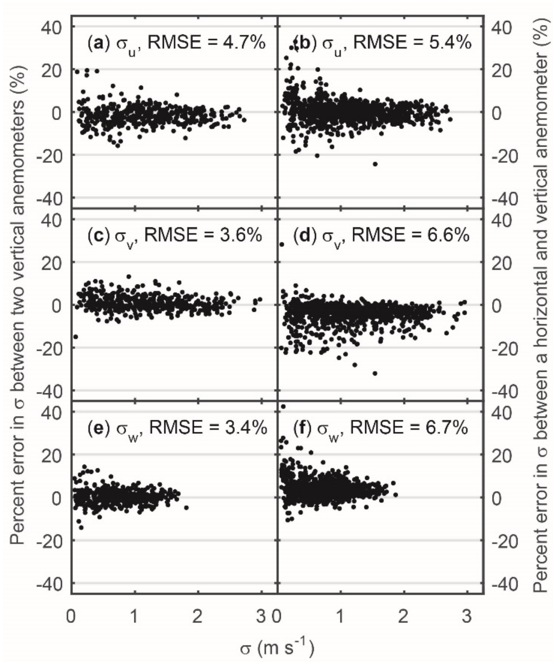

Fig. 4. Kaimal corrected measurements (i.e. one of three priors tested) of the 5-minute standard deviation of wind (σ) along the cardinal (**a, b**) u, (**c, d**) v, and (**e, f**) w axes are more equivalent between vertically and horizontally mounted sonic anemometers. The percent errors between a horizontal and a vertical anemometer (**b**, **d**, **f**) are smaller for all three cardinal dimensions than it was for the uncorrected data (Fig. 2) being more similar to those found between two anemometers mounted vertically (**a**, **c**, **e**). The data are from 2011 and 2013 field experiments at the GLEES AmeriFlux site (Frank et al., 2016; Frank et al., 2013). The 2011 data in panels **b**, **d**, and **f** are randomly paired between the two anemometers in different orientations. Results are summarized as root mean square error (RMSE).

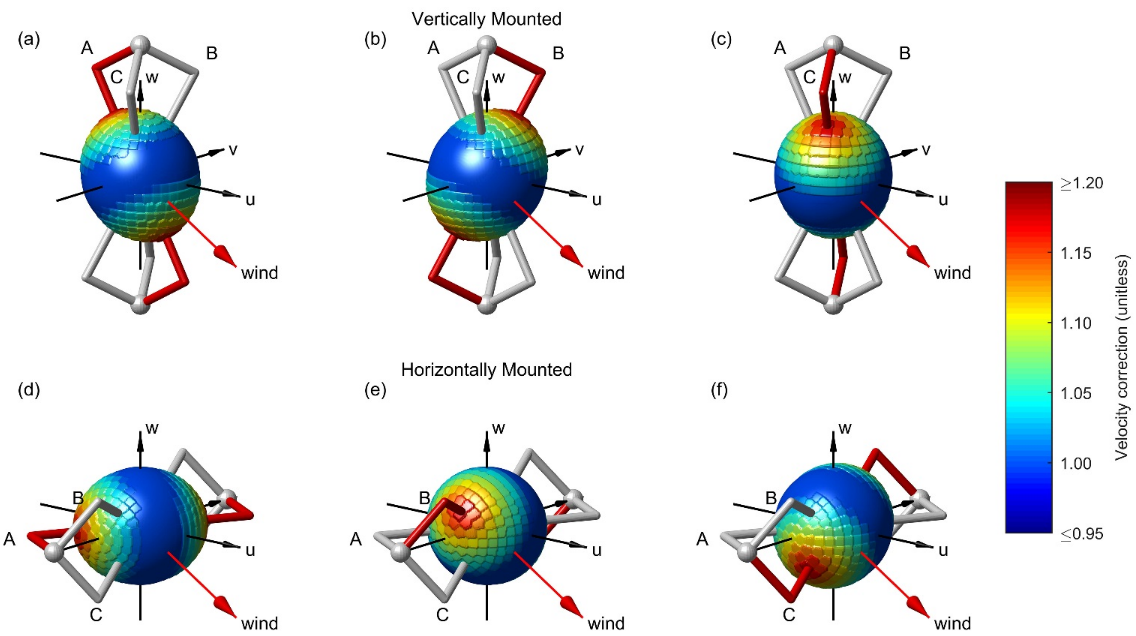

Fig. 5. The Kaimal correction, one of three priors tested in this study, evaluated among 512 cells for the (**a, d**) A, (**b, e**) B, and (**c, f**) C transducer pairs of the CSAT3 sonic anemometer mounted either in the (**a-c**) typically vertical or (**d-f**) experimentally horizontal orientations. Though the correction is identical relative to all transducer pairs, the same instantaneous wind results in different corrections depending on the transducer pair and the orientation.

Atmos. Meas. Tech. Discuss., doi:10.5194/amt-2016-145, 2016
Manuscript under review for journal Atmos. Meas. Tech.
Published: 23 June 2016

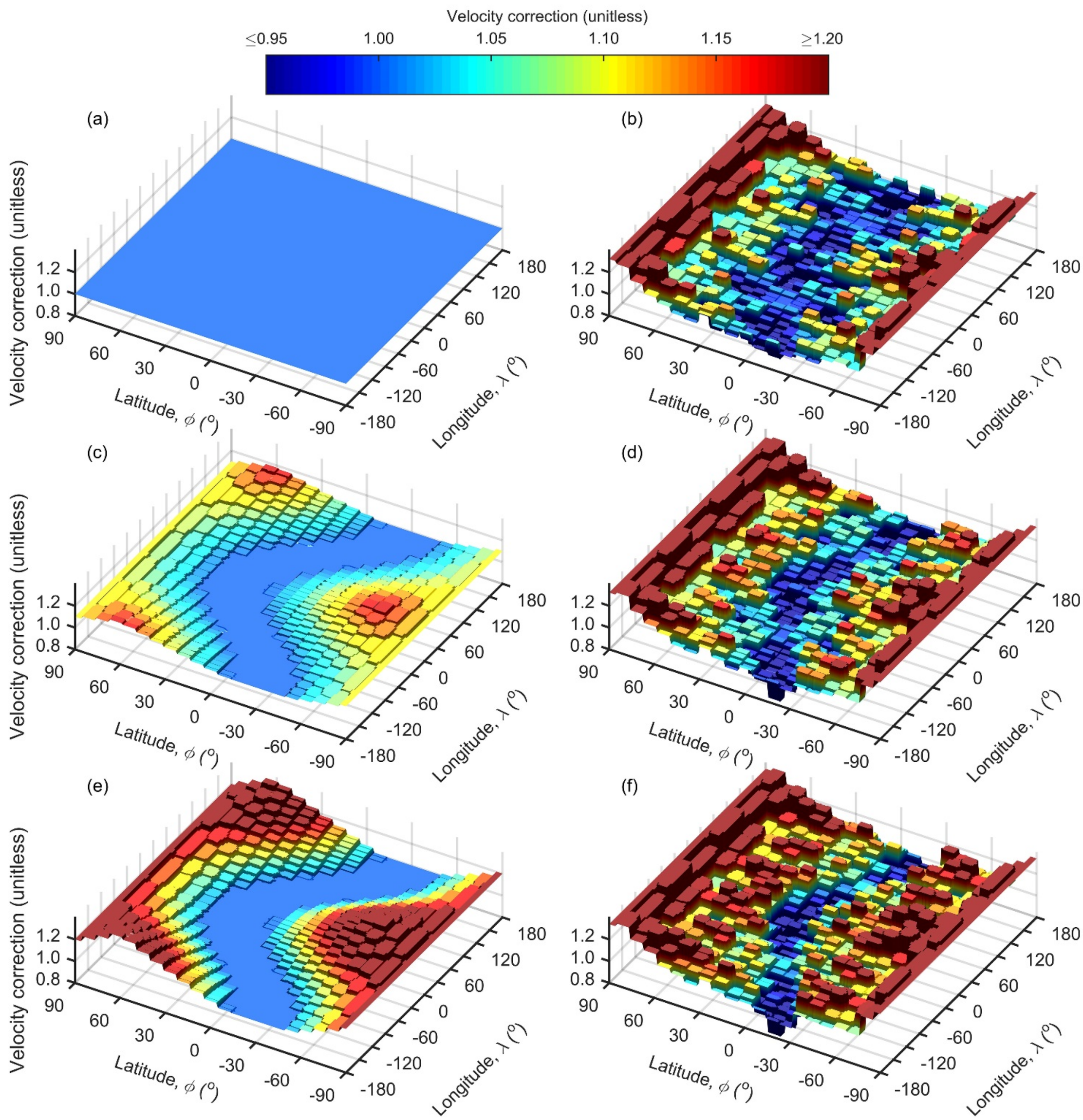

Fig. 6. The A transducer pair correction evaluated among 512 cells for the three prior corrections tested in this study, (**a**) flat, (**c**) Kaimal, and (**e**) double-Kaimal, with their corresponding unnormalized posterior corrections (**b**), (**d**), and (**f**), respectively. All posteriors have similar relative topography. They differ in absolute scaling where priors with higher absolute magnitude

Atmos. Meas. Tech. Discuss., doi:10.5194/amt-2016-145, 2016
Manuscript under review for journal Atmos. Meas. Tech.
Published: 23 June 2016

result in posteriors with higher absolute magnitude, which is apparent from the different colorings.

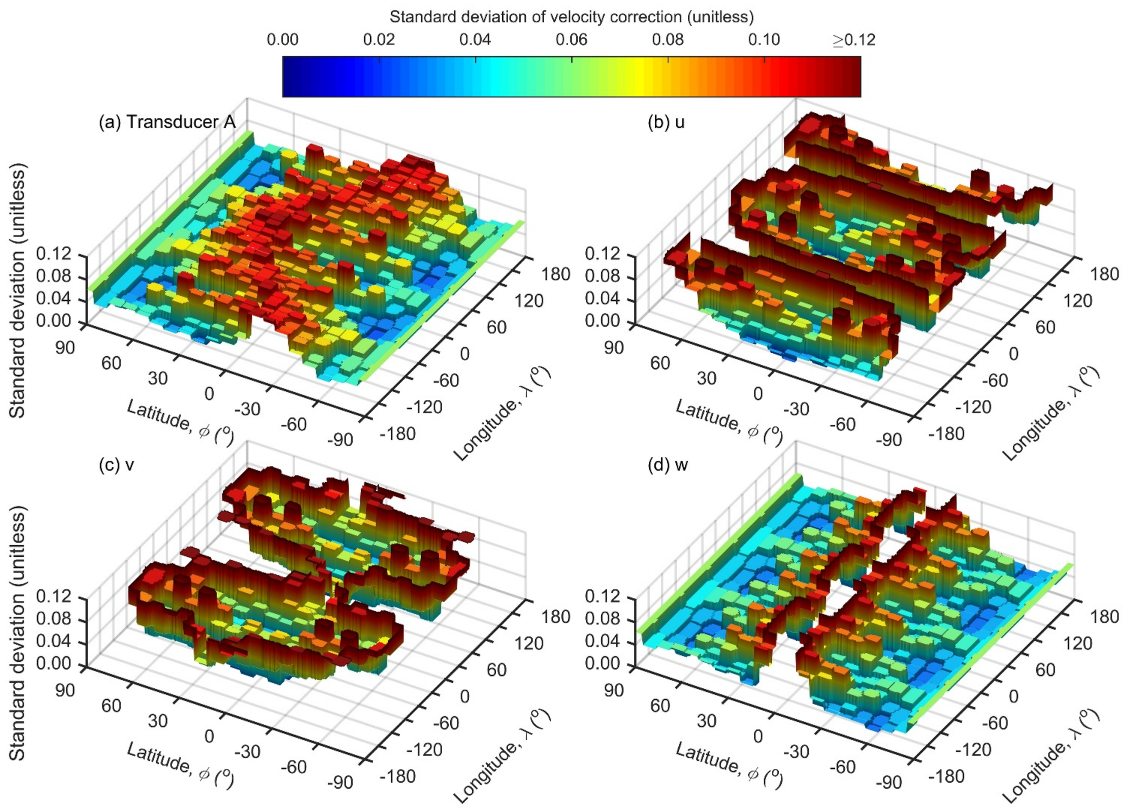

Fig. 7. Standard deviations of the posterior correction for (**a**) the A transducer pair and the wind velocities (**b**) *u*, (**c**) *v*, and (**d**) *w*. When compared to the standard deviation of the prior which was defined as 0.1, the transducer correction is more certain in regions with higher topography (Fig. 6). The results in CSAT3 sonic coordinates reflect both the uncertainty in the transducer correction plus cancelation and amplification of errors due to the coordinate transformation. The posterior correction for *u*, *v*, and *w* is most certain for winds along the *u*, *v*, and *w*-axes, respectively.

Atmos. Meas. Tech. Discuss., doi:10.5194/amt-2016-145, 2016
Manuscript under review for journal Atmos. Meas. Tech.
Published: 23 June 2016

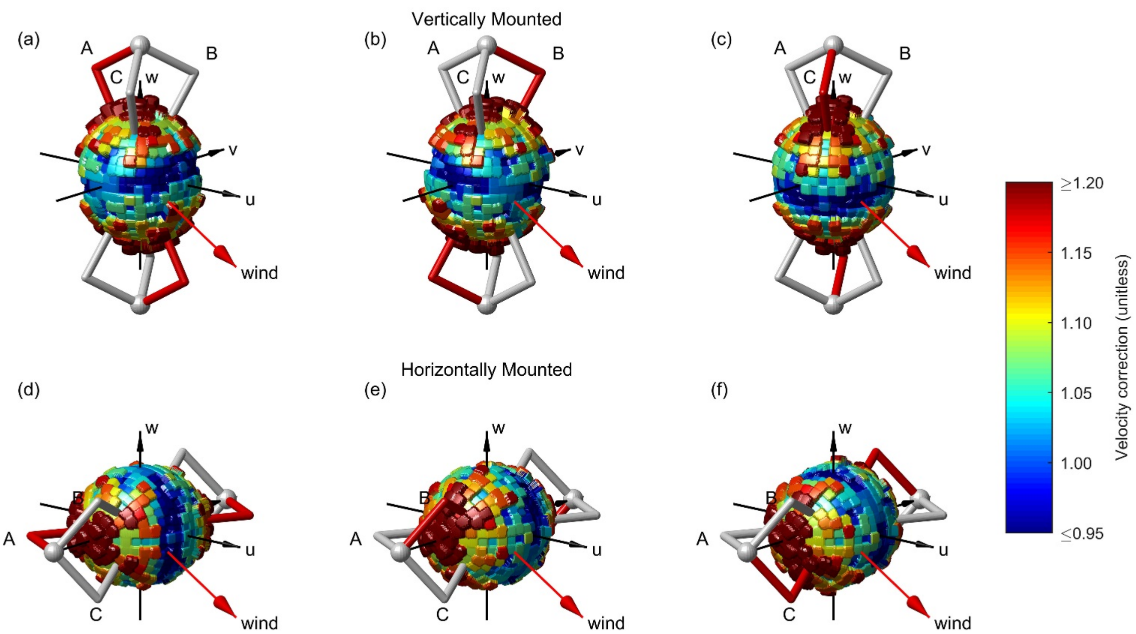

Fig. 8. The posterior correction evaluated for the (**a, d**) A, (**b, e)** B, and (**c, f**) C transducer pairs of the CSAT3 sonic anemometer mounted either in the (**a-c**) typically vertical or (**d-f**) experimentally horizontal orientations. The correction is identical relative to all transducer pairs and is constructed from 512 cells with 138 unique values. The Bayesian model adjusts these values to simulataneously correct the same instantaneous wind measured from different transducer pairs and orientations in order to produce similar cardinal *u*, *v*, and *w* wind statistics (Fig. 10).

Atmos. Meas. Tech. Discuss., doi:10.5194/amt-2016-145, 2016
Manuscript under review for journal Atmos. Meas. Tech.
Published: 23 June 2016

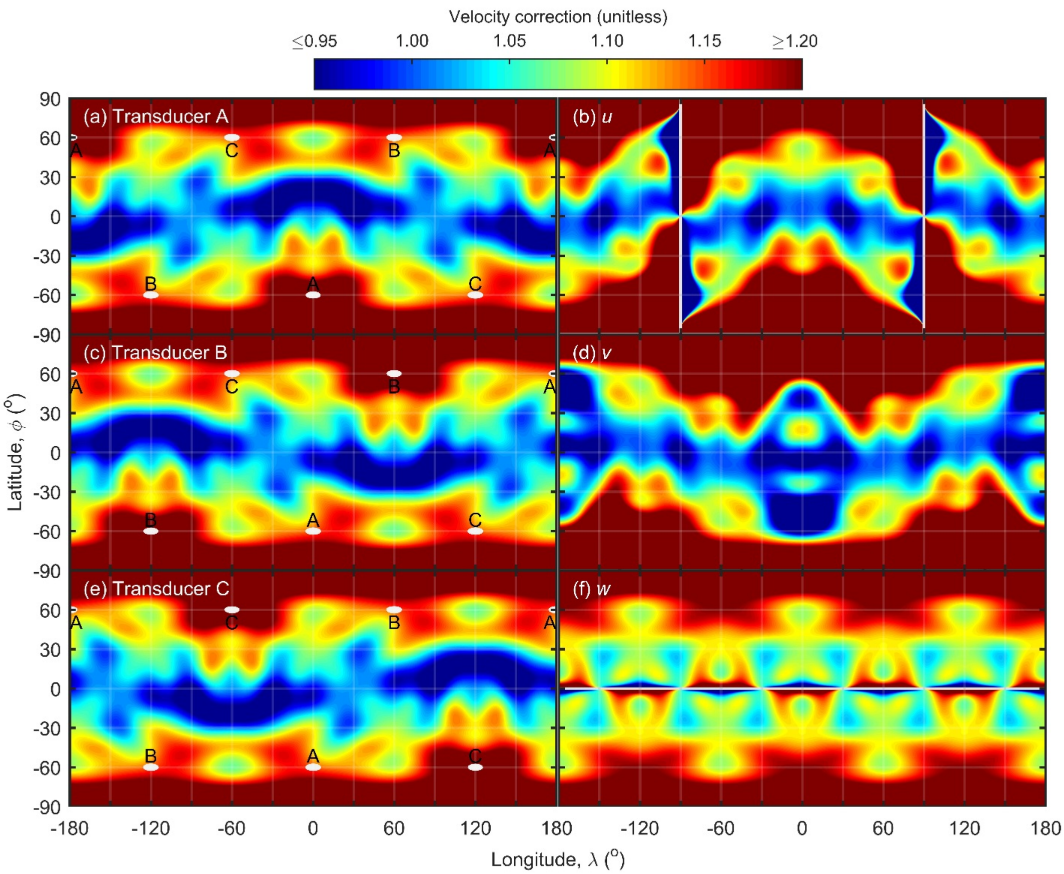

Fig. 9. The posterior correction for the (**a**) A, (**c**) B, and (**e**) C transducer pairs, each represented by a white dot, of a CSAT3 sonic anemometer accounts for both self-shadowing and cross-shadowing between transducers. The same correction expressed in sonic anemometer coordinates (**b**) *u*, (**d**) *v*, and (**f**) *w* shows that for near-equatorial winds, minimal correction is required for the horizontal wind components while even more correction exists in the vertical wind component *w* than was present with the Kaimal correction (Fig. 3f). Longitude and latitude are relative to the *u* axis (Fig. 1).

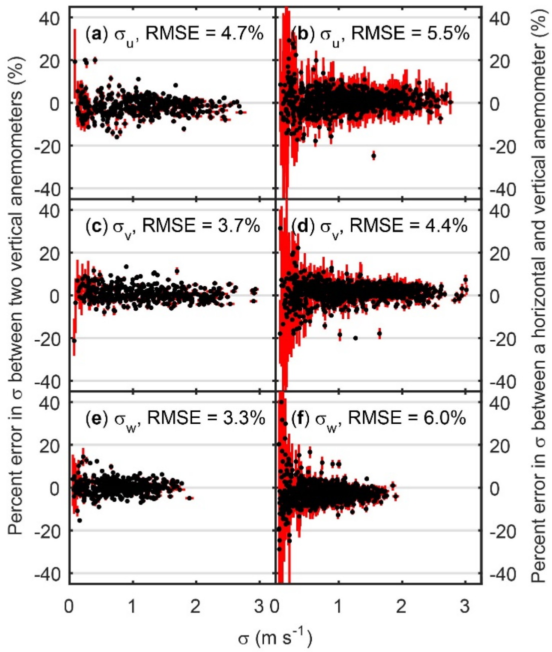

Fig. 10. Posterior corrected measurements of the 5-minute standard deviation of wind (σ) along the cardinal (**a, b**) *u*, (**c, d**) *v*, and (**e, f**) *w* axes are most equivalent between vertically and horizontally mounted sonic anemometers than with either the uncorrected (Fig. 2) or Kaimal corrected data (Fig. 4). The percent errors between a horizontal and a vertical anemometer are small (**b**, **d**, **f**), especially for the cardinal *v*-dimension (**d**), and are similar to those found between two anemometers mounted vertically (**a**, **c**, **e**). The data are from 2011 and 2013 field experiments at the GLEES AmeriFlux site (Frank et al., 2016; Frank et al., 2013). The 2011 data in panels **b**, **d**, and **f** are randomly paired between the two anemometers in different orientations. Results are summarized as root mean square error (RMSE). The red lines are 95% credible intervals.

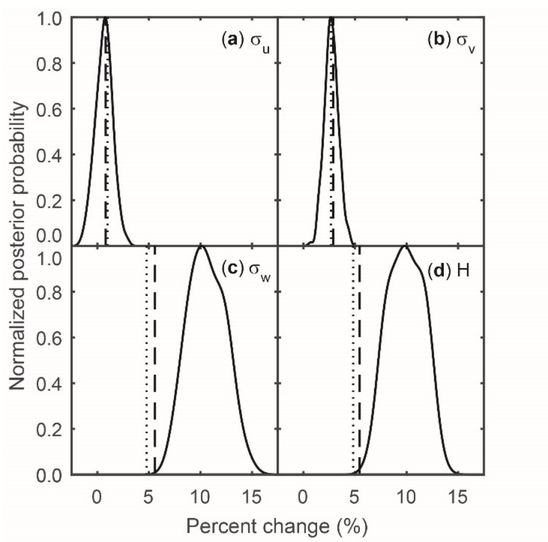

Fig. 11. Though application of the Kaimal (dashed lines) and posterior (solid lines) corrections result in similar changes to the 5-minute standard deviations of wind (σ) along the (**a**) *u* and (**b**) *v* axes, application of the posterior correction results in significantly higher (95% credible interval) (**c**) winds along the *w* axis and (**d**) sensible heat flux (*H*). The dotted lines are an alternate formulation of the Kaimal correction proposed by Wyngaard and Zhang (1985) and used in Horst et al. (2015). Data are for vertically mounted anemometers only.